ELSEVIER

Contents lists available at ScienceDirect

Geochimica et Cosmochimica Acta

journal homepage: www.elsevier.com/locate/gca





Constraining sulfur incorporation in calcite using inorganic precipitation experiments

Szabina Karancz^{a,*}, Joji Uchikawa^b, Lennart J. de Nooijer^a, Mariëtte Wolthers^c, Kyle A. Conner^b, Corinne G. Hite^b, Richard E. Zeebe^b, Shiv K. Sharma^b, Gert-Jan Reichart^{a,c}

- ^a Department of Ocean Systems, NIOZ-Royal Netherlands Institute for Sea Research, Texel, the Netherlands
- ^b Department of Oceanography, SOEST, University of Hawaii at Manoa, Honolulu, HI, USA
- ^c Department of Earth Sciences, Utrecht University, Utrecht, the Netherlands

ARTICLE INFO

Associate editor: Nicola Allison

Keywords: Calcite growth experiment Sulfate incorporation Ion-pair formation Inorganic carbon chemistry Proxy

ABSTRACT

The sulfur over calcium ratio (S/Ca) in foraminiferal shells was recently proposed as a new and independent proxy for reconstructing marine inorganic carbon chemistry. This new approach assumes that sulfur is incorporated into CaCO₃ predominantly in the form of sulfate (SO₄²) through lattice substitution for carbonate ions (CO_3^2) , and that S/Ca thus reflects seawater $[CO_3^2]$. Although foraminiferal growth experiments validated this approach, field studies showed controversial results suggesting that the potential impact of [CO3-7] may be overwritten by one or more parameters. Hence, to better understand the inorganic processes involved, we here investigate S/Ca values in inorganically precipitated CaCO₃ (S/Ca_(cc)) grown in solutions of CaCl₂ - Na₂CO₃ -Na₂SO₄ - B(OH)₃ - MgCl₂. Experimental results indicate the dependence of sulfate partitioning in CaCO₃ on the carbon chemistry via changing pH and suggest that faster precipitation rates increase the partition coefficient for sulfur. The S/Ca ratios of our inorganic calcite samples show positive correlation with modelled $[CaSO_4^0]_{(a0)}$, but not with the concentration of free SO_4^{2-} ions. This challenges the traditional model for sulfate incorporation in calcite and implies that the uptake of sulfate potentially occurs via ion-ion pairs rather than being incorporated as single anions. Based on the [Ca²⁺] dependence via speciation, we here suggest a critical evaluation of this potential proxy. As sulfate complexation seems to control sulfate uptake in inorganic calcite, application as a proxy using foraminiferal calcite may be limited to periods for which seawater chemistry is well-constrained. As foraminiferal calcite growth is modulated by inward Ca²⁺ flow to the site of calcification coupled to outward H⁺ pumping, sulfate incorporation as CaSO₄ ion-pair in the foraminifer's shell also provides a mechanistic link for the observed relationship between $S/Ca_{(cc)}$ and $[CO_3^2]$.

1. Introduction

Models predicting the consequences of ongoing greenhouse gas emissions rely on our ability to reconstruct past climatic conditions, such as quantifying the response of global temperature to changes in atmospheric pCO_2 . Therefore, reliable proxies for past seawater temperature (e.g., Dekens et al., 2008; Laepple and Huybers, 2013) and for CO_2 (e.g., Martinez-Boti et al., 2015; Palmer et al., 2010; Zhou et al., 2020) are of critical importance. The reconstruction of past pCO_2 is mostly based on estimating past seawater inorganic carbon chemistry, assuming equilibrium partitioning between the ocean and atmosphere.

Due to their widespread occurrence, foraminifera, a group of

unicellular carbonate-shelled protists, are one of the most utilized archives for past ocean conditions. The isotopic composition of their calcite in particular provide popular reconstruction tools: the δ^{18} O values of fossilized tests enable reconstruction of temperature and salinity (e.g., Bemis et al., 1998; Epstein et al., 1953), while δ^{11} B values are used to reconstruct past seawater pH (e.g., Foster, 2008; Hemming and Hanson, 1992). Minor and trace elements incorporated by the foraminifer during shell calcification also reflect seawater conditions at the moment of calcite precipitation, e.g., the incorporation of Mg reflects temperature (Anand et al., 2003; Lea et al., 1999; Rosenthal et al., 2000). Also, marine carbon chemistry has been shown to influence the uptake of elements like B (Allen and Hönisch, 2012; Allen et al., 2012;

E-mail address: szabina.karancz@nioz.nl (S. Karancz).

^{*} Corresponding author at: Department of Ocean Systems, NIOZ-Royal Netherlands Institute for Sea Research, Landsdiep 4, 1797 SZ 't Horntje (Texel), the Netherlands.

Haynes et al., 2017; Yu and Elderfield, 2007; Yu et al., 2007), Sr (Keul et al., 2017; Russell et al., 2004), U (Keul et al., 2013; Raitzsch et al., 2011) in carbonate shells.

Ideally, any of these proxies would be sensitive to only one of the marine inorganic carbon system parameters: $p\text{CO}_2$, $[\text{CO}_3^2]_{(\text{total})}$, $[\text{HCO}_3]_{(\text{total})}$, dissolved inorganic carbon concentration ([DIC]), pH, or total alkalinity. If the effect of temperature (T), salinity (S), and the element's concentration in seawater can be accounted for, two of such proxies can be used to reconstruct the complete marine inorganic carbon system and hence, atmospheric $p\text{CO}_2$. However, this is usually not the case, as these parameters often covary and proxies may be affected by more than one parameter as best exemplified by the boron over calcium ratio (B/Ca; e.g., Allen et al., 2012; Babila et al., 2014; Evans et al., 2016; Gray and Evans, 2019; Gray et al., 2018; Guo et al., 2019; Henehan et al., 2015). Therefore, there is a strong need for novel proxies specific to marine carbonate system parameters.

The foraminiferal sulfur over calcium ratio (S/Ca_(cc)) could serve as a potential proxy for dissolved carbonate ion concentration (Van Dijk et al., 2017). The S/Ca_(cc) carbonate system proxy is based on results from cultured benthic foraminifera, which showed higher sulfur incorporation into their shells at lower seawater [CO₃²⁻]_(total) (Van Dijk et al., 2017). As the main form of sulfur incorporated into the shells of foraminifera is sulfate anion (SO_4^{2-}) and it is thought to substitute for CO_3^{2-} (Busenberg and Plummer, 1985; Pingitore et al., 1995; Takano, 1985), S/Ca_(cc) became one of the candidates for reconstructing past changes in the marine inorganic carbon system. However, it has been observed for other incorporated elements that calibrations based on culture experiments and core-top studies are not always in complete agreement (see e. g., Henehan et al., 2015 for B/Ca). Data obtained from field surveys often show covariance between multiple environmental parameters (e. g., [CO₃²]_(total) and pH), which may reflect the natural covariance within the carbonate system. Since this covariance is inherent to the oceanic carbonate system, these effects can be deconvolved only through wellconstrained culturing experiments in which the carbonate system is manipulated. In addition to the multiple environmental impacts, element incorporation in foraminiferal calcite can also be affected by biological processes (i.e., the vital effect; de Nooijer et al., 2014; Erez, 2003), which could result in multiple factors impacting a proxy. Biology will partially control the conditions at the site of calcification, influencing the calcite precipitation rate (R) via additional kinetic controls and consequently, element incorporation (Geerken et al., 2022).

It is crucial to understand such processes when the foraminifer's element/calcium (El/Ca_(cc)) ratios are evaluated, but even more fundamentally, basic chemical dependencies of El/Ca_(cc) ratios in calcite need to be well-constrained. For instance, it is suggested that some elements may inhibit or enhance the uptake of other elements due to their crystallographic distortion of the calcite lattice (Davis et al., 2004; Mewes et al., 2015; Meyer, 1984; Nielsen et al., 2013; Nielsen et al., 2016). This includes Mg²⁺ that, while substituting for Ca²⁺ during calcite precipitation, causes a shrinkage in the crystal lattice due to the difference in their ionic radius (Evans, 1966; Maslen et al., 1995). Van Dijk et al., (2019a) similarly suggested that the incorporation of sulfate may be enhanced by the increase in the calcite's Mg/Ca based on their co-distribution in the calcite banding of the foraminifera shell. Furthermore, Uchikawa et al. (2023) found an impact of SO₄² on the kinetics of CaCO₃ precipitation and an increase in the incorporation of B $(OH)_4^-$ in the calcite with increasing solution $[SO_4^{2-}]_{(total)}$. Stretched calcite unit cells due to the large ionic radius of SO_4^{2-} anion may provide space for the incorporation of B(OH)⁻₄ or other ions with a size larger than the CO_3^{2-} anion. This substitution mechanism is referred to as the "cooperative incorporation" of elements.

These observations and potential linkages motivated us to investigate how solution chemistry impacts S/Ca ratios during inorganic calcite growth experiments. Therefore, to improve our understanding of the role of carbon chemistry on incorporation of S into CaCO₃, we performed calcite growth experiments with constant total sulfate concentration

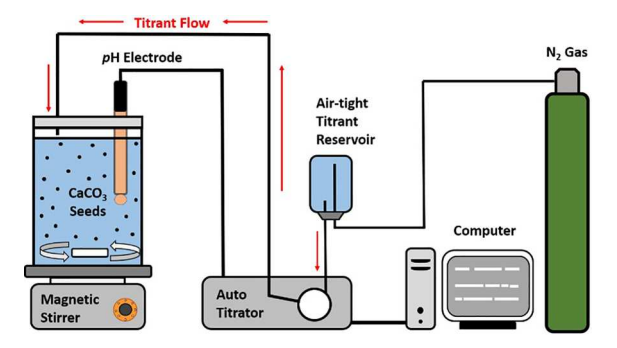


Fig. 1. The experimental set-up (pH-stat system) modified after Fig. 2 in Uchikawa et al. (2015). The reaction chamber is placed on a magnetic stirrer and connected to the custom-built titrator (Zeebe and Sanyal, 2002) via the pH electrode. All experiments were performed at near-constant room temperature, hence additional temperature control was not applied as during the experiments of Uchikawa et al. (2015). The total internal volume of the reactor is approximately 1.06 L. After placement of 1.00 L of experimental solution, the pH electrode, and a suspended magnetic stir bar (Nalgen), the reactor had minimal headspace (approximately 32 mL) that was practically negligible for significant gas exchange with the experimental solution.

 $([SO_4^{2-}]_{(total)})$ at varying carbonate system conditions. In addition to the primary question of this study, we assessed causal relationships between incorporation of different ions $(Mg^{2+},\ B(OH)_4^-,\ Na^+).$ As described above, $Mg/Ca_{(cc)}$ and $B/Ca_{(cc)}$ ratios in the calcite may affect SO_4^{2-} incorporation via cooperative incorporation, which would have consequences for the application of these individual elements (El/Ca_{(cc)} ratios) in carbon system reconstructions. As the influence of the precipitation rate can potentially mask a primary control of the carbon system (Busenberg and Plummer, 1985), we measured Na $^+$ concentration in the calcite, which is shown to vary with calcite growth rate (Devriendt et al., 2021), and explored relationships between SO_4^{2-} and Na^+ incorporation.

2. Methods

2.1. Experimental set-up

Four sets of calcite growth experiments under various carbon chemistry and precipitation rate conditions were performed to investigate the primary controls on sulfate incorporation. These experiments followed the approach described in Uchikawa et al. (2015). Briefly, calcite growth took place in a reaction chamber isolated from the ambient laboratory air (Fig. 1). A pH electrode (Thermo Scientific Orion 8172BNWP ROSS Sure-Flow) sent voltage readings of the experimental solution to the titrator system and signaled for the addition of titrant upon a decrease of 0.01 unit from the pre-specified solution pH_{NBS} value. A calibration of the pH electrode was done prior to each experimental run by NIST pH buffers (pH 4.01, 7.00, 10.01; Thermo Scientific Orion) with an equilibration time of \sim 9 min for each buffer. The titration system dosed 0.3 M solutions of NaOH and Na₂CO₃ in increments of 20 μL during the pH adjustment and precipitation phase, respectively. The titrant was dosed to the solution through ports located on top of the reactor. All titrant solutions were prepared in a glove-bag under an N2 atmosphere and stored in plastic HDPE serum vials sealed with rubber stoppers and aluminum covers until the start of the experiment. Following the seeded overgrowth technique, calcite seeds (Sigma-Aldrich #310034) were added to the solution at the start of the experiment to initiate the calcite precipitation (Sanyal et al., 2000; Uchikawa et al., 2015; Zeebe and Sanyal, 2002). As observed in previous studies (Uchikawa et al., 2015; 2017; 2023), the isotopic composition of the seeds was homogenous ($\delta^{13}C = -17.91 \pm 0.04$ %; $\delta^{18}O = -20.67 \pm 0.04$ 0.05 %; 1 σ SD; n = 5) and contained only minor amounts of S (0.03 \pm 0.01 mmol mol $^{-1}$; 1 σ SD; n = 3), B (0.10 \pm 0.16 μmol mol $^{-1}$; 1 σ SD; n = ÷

Summary of experimental conditions, including temperature (T), pH_{NBS}, total concentrations of dissolved inorganic carbon ([DIC]), bicarbonate ion ([HCO3]_(roall), carbonate ion ([CO3]_(roall)), calcium ([Ca²-¹₁/_(roall)) sulfate ([SO₄²]_(rotal)), calcite saturation state (Ω), salinity (S), and aqueous sulfate speciation ([SO₄²]_(aa), [CaSO₄]_(laa), [MgSO₄]_(aa), [NaSO₄]_(aa). Instribution of sulfate speciation was calculated in PHREEQC (Version

Experimental series	Conditions	T C	pH (NBS)	[DIC] µmol kg ⁻¹	$\rm [HCO_3^-]_{(total)}$ $\mu mol~kg^{-1}$	$[\mathrm{CO_3^{2-1}}]_{(total)}$ $\mu mol~kg^{-1}$	$[\mathrm{Ca}^{2+}]_{(\mathrm{total})}$ mmol k g^{-1}	$[\mathrm{SO_4^{2-}}]_{(\mathrm{total})}$ mmol kg^{-1}	Ω	S	$[\mathrm{SO}_4^2]_{\mathrm{(aq)}}$	$[{ m CaSO}_4^0]_{ m (aq)}$	$[{ m MgSO_4^0}]_{ m (aq)}$	$[\mathrm{NaSO_4^-}]_{\mathrm{(aq)}}$
[DIC]	A	23	8.205	1500	1343	104	11	4.5	10.7	1.9		25 %	% 9	2 %
	В	23	8.205	2400	2150	165	11	4.5	17.0	1.9	% 89	25 %	% 9	2%
	C	23	8.205	2800	2508	193	11	4.5	19.5	1.9	% 89	24 %	% 9	2 %
	О	23	8.205	3200	2867	219	11	4.5	22.4	2.0	% 89	24 %	% 9	2 %
22+	<	ç	9000	0000	2030	170	6	п .	7	1	70 09	70 00	70 9	70 00
[رم]	ζ ε	3 5	9.203	2800	2220	1/3	C		10.1); ;	02.60		0.00	0, 0
	р	72	8.205	7800	2208	193	11	t.5	19.5	1.9	% 80	24 %	% 0	7%
	O	23	8.205	2800	2485	219	13.5	4.5	22.9	2.2	% 99	27 %	2 %	2 %
[DIC]-[Ca ²⁺]	Ą	23	8.205	2200	1959	165	12.5	4.5	17.0	2.1	% 99	26 %	2 %	2 %
	В	23	8.205	2400	2150	165	11	4.5	17.0	1.9		25 %	% 9	2%
	C	23	8.205	2800	2526	173	9.3	4.5	17.0	1.7	% 69	22 %	% 9	2 %
	D	23	8.205	3200	2903	179	∞	4.5	17.0	1.6	71 %	20 %	% 9	3 %
2+2			1			ļ	į							ě
$pH-[Ca^{-+}]$	0	53	7.955	2400	2110	157	24	4.5	17.0	3.4		35 %	% 4	2%
	Α	23	8.050	2400	2128	159	17.5	4.5	17.0	5.6		31 %	2 %	2%
	В	23	8.205	2400	2150	165	11	4.5	17.0	1.9	% 89		% 9	2 %
	C	23	8.350	2400	2158	178	7.5	4.5	17.0	1.5		19 %	2 %	2 %

3), and Na (0.01 \pm 0.01 mmol mol⁻¹; 1 σ SD; n = 3). For Mg, the potential offset to Mg associated with the seeds is somewhat larger (0.56 \pm 0.01 mmol mol⁻¹; 1σ SD; n = 3). The initial seeds and the final precipitated samples were weighed on a high-precision balance before and after the experimental runs, which theoretically allows for constraining the overgrowth fraction. However, potential loss of sample can occur during both seed addition to the parent solution as well as during the collection of the final precipitates, and therefore ¹³C-spike was used to provide a separate constraint on the overgrowth. The Na₂CO₃ solutions used as the titrant and as the DIC source for the experimental solutions were spiked with ^{13}C to $\delta^{13}\text{C}_{VPDB} = +76 \pm 0.80$ % and a mass balance equation was used to calculate the amount of carbonate added during the experiment and subsequently the El/Ca ratios of the overgrowth (see Uchikawa et al., 2015). Note that El/Ca ratios measured on our samples (seeds and overgrowth contribution) were higher than those of the seeds by at least an order of magnitude. Hence, the residual El/Ca ratios and their heterogeneities confirmed for the seeds were insignificant for our ¹³C mass balance approach to constrain the El/Ca ratios of the overgrowth.

2.2. Solution chemistry and experimental procedures

Parent solutions were prepared to 1 L as CaCl₂ - Na₂CO₃ - Na₂SO₄ -MgCl₂ – B(OH)₃ solution. First B(OH)₃, and Na₂SO₄ were gravimetrically added to and dissolved in Milli-Q ultra-pure deionized water in a plastic volumetric flask. To ensure a CO₂-free solution, the deionized water was bubbled with N₂ gas before use and during the addition to the chemicals. Next, CaCl2 and MgCl2 were volumetrically added from stock solutions of known Ca²⁺ and Mg²⁺ concentration, and the headspace of the volumetric flask was purged with N2 several times during the preparation of the parent solution. The DIC source was added last, after which the volume of the solution was brought to 1 L with N2 gas bubbled deionized water. The DIC solution was prepared in a N2 glove bag with the dilution of ¹³C-spiked 0.3 M Na₂CO₃ stock solution. To avoid instantaneous calcite precipitation in the parent solution, 1 M HCl was added to convert CO₃²⁻ to HCO₃ by lowering pH. All experiments were performed at room temperature (23 \pm 0.3 °C; $\pm 1\sigma$ SD).

Solution chemistry was designed for four sets of experiments, each with constant concentrations of sulfur (4.5 mmol kg⁻¹), boron (1.68 mmol kg⁻¹) and magnesium (2.0 mmol kg⁻¹). Their experimental settings and scopes were as follows:

#1) The [DIC] experimental series varied [DIC] between 1.5 and 3.2 mM to quantify the overall impact of changing carbonate chemistry on the incorporation of sulfur, boron, magnesium and sodium. Due to the changes applied to [DIC], there were concurrent and consequential shifts in $[CO_3^2]$, $[HCO_3]$ and calcite saturation state (Ω) as well, where Ω is defined as the ratio of $[CO_3^{2-}][Ca^{2+}]$ to the calcite solubility product (K_{sp}^*) . However, we here derived Ω from the saturation index as described below.

#2) The [Ca $^{2+}$] experiment series employed solutions with total concentration of Ca²⁺ ([Ca²⁺]_(total)) ranging from 9.30 to 13.5 mM, while keeping [DIC] and pH constant. This resulted in increasing Ω with increasing [Ca²⁺]_(total).

#3) In the [DIC]-[Ca²⁺] experiments, the range of [DIC] was varied from 1.5 to 3.2 mM, while 7.5 to 17.5 mM of [Ca²⁺]_(total) was added to maintain a constant Ω for these experiments.

#4) The pH-[Ca²⁺] experiments were designed likewise to keep constant Ω values, but this time with an adjustment in pH_{NBS} between 7.995 and 8.350 and with corresponding variation in [Ca²⁺]_(total) between 7.5 and 24 mM. As the first three experimental series (#1 to #3) were performed at a constant pH, this last series was designed to investigate the effect of pH on S/Ca (Table 1).

Changes in Ω and precipitation rate are naturally coupled. Therefore, the first two experiments monitored the impact of calcite precipitation kinetics on sulfate incorporation, while the third and fourth experiments maintained a constant R, thereby isolating the effect of carbon chemistry on element incorporation. The solutions for inorganic calcite precipitation were precisely prepared to these pre-planned experimental conditions (Table 1), and each experimental condition was repeated three times

After mixing and dissolving all the salts described above, the solutions were brought up to the pH values required for the planned experiments (see above) by titration with 0.3 M NaOH. After solution pH stabilized at the experimental value, the titrant was changed to 0.3 M $^{13}\text{C-spiked Na}_2\text{CO}_3$ and the pH was let to equilibrate for another 5 min before 40 mg of pre-weighed calcite seeds were added. Sensitivity of pH_{NBS} changes due to CaCO₃ precipitation and Na₂CO₃ dosage during the titration depends on chemical composition and buffering capacity of the experimental solutions. Variations in pH_{NBS} were contained less than ± 0.007 range (1 σ SD of all pH_{NBS} readings in a given experiment). The experiment was terminated when the amount of calcite overgrowth approximately doubled the original calcite mass added as the seeds, which was estimated based on the titrated volume of the 0.3 M ¹³Cspiked Na₂CO₃. The calcite samples were separated from parent solution by vacuum filtration through 0.2 µm membrane filters and rinsed with deionized water. The samples were dried for at least 24 h at 65 °C, collected, and stored until geochemical analyses.

The titration with Na₂CO₃ solution was used to counteract the decrease in solution pH, [DIC], and total alkalinity due to calcite precipitation. However, such replenishment for the drawdown of Ca²⁺ was not possible in our experimental system. Nevertheless, based on the mass gain of the overgrowth fraction and the total moles of Ca²⁺ initially present in the growth solution, the estimates for the total loss of Ca²⁺ from the solution due to calcite precipitation were only on the order of 2–8 %. We also observed that the pace of titrant dosing remained practically constant, based on which we expect no appreciable impact on the precipitation rate by the gradual Ca²⁺ drawdown. While calcite precipitated, other ions (Mg²⁺, SO₄²⁻, B) were also withdrawn from the growth solution, but due to their very small contribution in the formed CaCO₃, reduction in their solution concentrations is negligible.

The precipitating solutions used for our experiments were simplified and more dilute compared to the standard seawater composition. Therefore, commonly applied programs such as CO2SYS (Lewis and Wallace, 1998) are not suited to calculate CO_2 speciation here. Instead, we used PHREEQC solution chemistry model with the phreeqc.dat database (Version 3; Parkhurst and Appelo, 1999) to determine the chemical species distribution in solution in terms of activities and molal concentrations. This model directly calculates molality of all carbon species, including both the free and complexed forms, and thus total concentrations of CO_3^{2-} and HCO_3^{-} ($[CO_3^{2-}]_{(total)}$, $[HCO_3^{-}]_{(total)}$, respectively), but concentrations of these species depend on combinations of factors and may not reflect changes in ionic strength of the solution.

By keeping [DIC] and pH constant upon solution preparation, one would intuitively expect no variation in $[CO_3^2]_{(total)}$ and $[HCO_3^2]_{(total)}$. However, changing the concentrations of cations that readily form complexes with CO_3^{2-} and HCO_3^{-} , such as aqueous Ca^{2+} ($[Ca^{2+}]_{(aq)}$), will contribute to a small variation in CO2-speciation. For instance, the increase of $[Ca^{2+}]_{(total)}$ from 9 to 14 mM in the $[Ca^{2+}]$ experiments at constant [DIC] (2.8 mM) and pH_{NBS} (8.205) results in 46 μ mol kg^{-1} increase in $[CO_3^2]_{(total)}$. Introducing more Ca^{2+} in the solution enhances formation of aqueous CaCO₃ and CaHCO₃ complexes and inevitably converts some of the CO2 to reestablish equilibrium. Within these experiments, CO₂-speciation will be affected by the Ca²⁺-speciation as the increase in ionic strength at constant [DIC] and pH would contribute to prominent change only in the activities of the CO2 species with minor influence on their concentrations. For a consistent approach, we used the activity-based calculations of $[\text{CO}_3^{2-}]_{(total)}$ and $[\text{HCO}_3^{-}]_{(total)}$ in all four sets of experiments. Species activities were taken from PHREEQC to calculate thermodynamic equilibrium constants for the dissociation of carbonic acid, which were afterwards translated into stoichiometric equilibrium constants using total activity coefficients as given by Zeebe and Tyrrell (2019). These stoichiometric constants were then applied to

compute total concentrations of CO_3^{2-} and HCO_3^{-} (Zeebe and Wolf-Gladrow, 2001). Errors associated with the computation of $[CO_3^{2-}]_{(total)}$ and $[HCO_3^{-}]_{(total)}$ were derived using 500 Monte Carlo simulations in Python (version 3.11.2; NumPy; Harris et al., 2020).

PHREEQC was also used to gain insight into the free sulfate anion concentration (i.e., $[SO_4^2]_{(aq)}$) and that of ion pairs such as MgSO $_4^0$ in the growth solution. Calcite saturation state (Ω) was determined from the saturation index (SI) calculated in PHREEQC using the logarithmic relation between SI and Ω .

2.3. $\delta^{13}C$ analysis to determine the overgrowth fraction

The carbon isotopic composition of the calcite samples was measured with a Kiel IV device coupled online to an isotope ratio mass spectrometer (IRMS, MAT 253 Thermo Fisher Scientific) at the Royal Netherlands Institute for Sea Research (NIOZ). Approximately 30 µg of calcite was pre-weighed, dissolved in orthophosphoric acid and analyzed at 71 °C. Analytical precision was determined by measuring the certified standard NBS-19 (1.98 \pm 0.04 ‰, \pm 1 σ SD, n = 11), and two additional standards, NBS-18 (-4.93 ± 0.07 ‰, $\pm 1\sigma$ SD, n = 11) and IAEA-603 (2.53 \pm 0.04 ‰, \pm 1 σ SD, n = 10), which provided quality control for the analysis. Instrumental drift was monitored by analyzing the NIOZ Foraminiferal in-House Standard (NFHS-1, 0.91 \pm 0.08 %, $\pm 1\sigma$ SD, n = 9; Mezger et al., 2016). As the samples are heavily 13 C-enriched (δ^{13} C ~ 35 %) relative to the standards and therefore somewhat removed from the standards in isotope space, duplicate measurements of the samples provided slightly poorer uncertainties for carbon compared to typical natural carbonates. The maximum standard deviation ($\pm 1\sigma$ SD) for duplicate analysis yielded an uncertainty of 0.89 % for δ^{13} C. Although this error is larger than the analytical uncertainty for environmental samples (which is approximately 0.07 ‰), it is still minor with respect to our purposes. Mass balance calculations indicate that even an offset of 1 % in δ^{13} C will impose only a 1 % error in the El/ Ca_(cc) ratios of the overgrowth fraction (Supplementary Figure S1).

2.4. Element/Ca analysis on newly grown calcite samples

The analysis of the inorganic calcite samples for B/Ca_(cc), Mg/Ca_(cc), Na/Ca_(cc), and S/Ca_(cc) was conducted at the NIOZ using a magnetic sector field inductively coupled plasma mass spectrometer (SF-ICP-MS, Thermo Fisher Scientific Element 2). About 0.5 mg of calcite was dissolved in 0.1 M HNO₃ (one-time in-house sub-boiled distilled grade, Nitric acid 68 %, AnalaR NORMAPUR®) and diluted for a Ca concentration of about 100 ppm. A low mass resolution (>300) was used to analyze isotopes of ¹¹B, ²³Na, and ²⁵Mg, whereas ³²S was measured in medium resolution (>4000) to resolve interferences with ¹⁶O¹⁶O (Van Dijk et al., 2017). All samples were measured against five ratio calibration standards (de Villiers et al., 2002) and an alternating order of the samples and using a 0.1 M HNO3 rinse provided efficient wash-out during the analytical run reducing potential carry-over. Three standards were used for quality control including NFHS-2-NP (Boer et al., 2022), JCp (Porites sp. coral), and JCt (Tridacna gigas giant clam, Okai et al., 2004). Additionally, NFHS-1 standard (Mezger et al., 2016) was used to scan and correct for instrumental drift. Internal precision on the individual measurements is $0.43 - 5.3 \,\mu\text{mol mol}^{-1}$ for ^{11}B , 0.0 - 0.018 mmol mol $^{-1}$ for ^{23}Na , 0.0 - 0.055 mmol mol $^{-1}$ for ^{25}Mg , and 0.0 - 0.28 mmol mol $^{-1}$ for ^{32}S . Reproducibility of the duplicate El/Ca_(cc) measurements on the samples were better than 0.015 mmol mol⁻¹ for B/ $Ca_{(cc)}$, 0.028 mmol mol⁻¹ for Na/Ca_(cc), 0.065 mmol mol⁻¹ for Mg/ $Ca_{(cc)}$, and 0.96 mmol mol⁻¹ for S/ $Ca_{(cc)}$, expressed here as two standard deviations ($\pm 2\sigma$ SD).

The measured $El/Ca_{(cc)}$ ratios were evaluated with respect to the carbon system parameters using least squares regression analysis. Significance test for linear regression provided validation for the observed relationships, where the results are expressed as p-values. Using the conventional threshold, relationships with p-value < 0.05 are

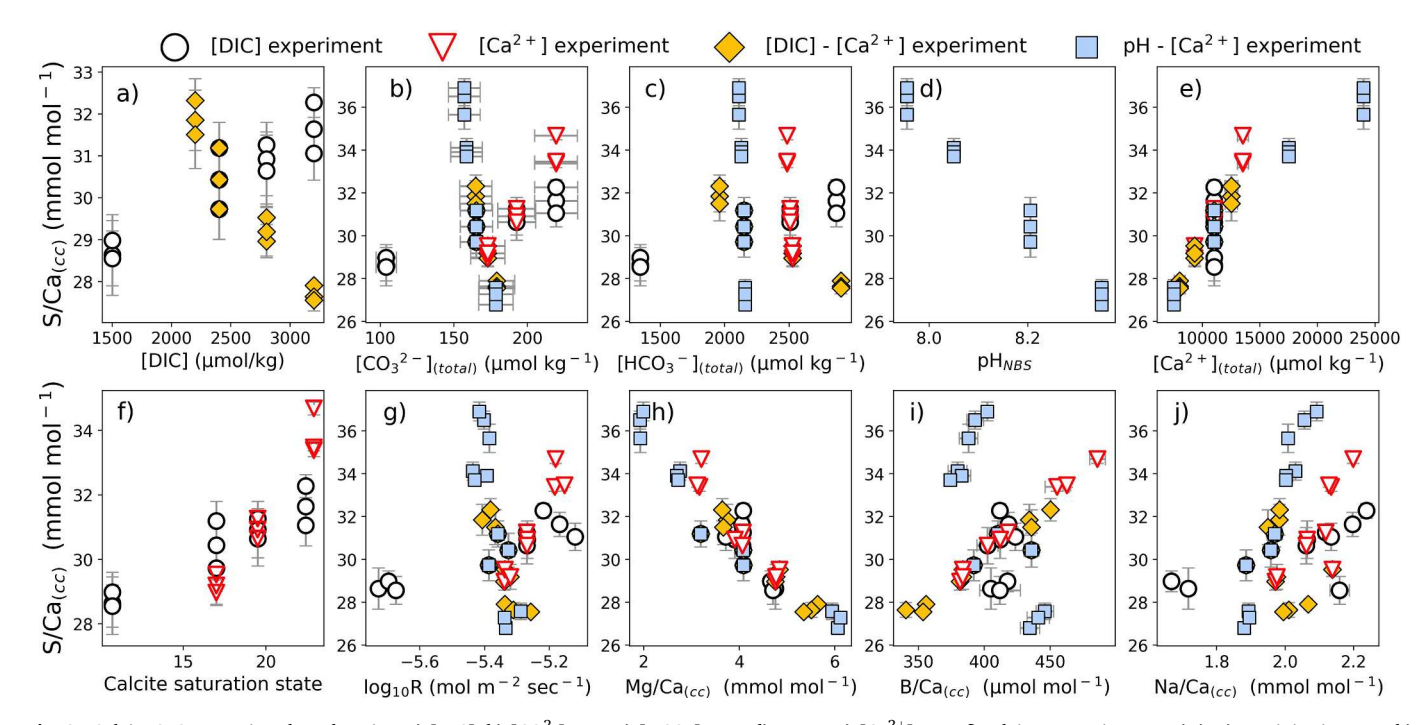


Fig. 2. Calcite S/Ca_(cc) ratios plotted against a) [DIC], b) $[CO_3^2]_{(total)}$, c) $[HCO_3^2]_{(total)}$, d) pH_{NBS} , e) $[Ca^{2+}]_{(total)}$, f) calcite saturation state (Ω) , g) precipitation rate, h) $Mg/Ca_{(cc)}$, and j) $Na/Ca_{(cc)}$, where the subscript $_{(total)}$ refers to the total concentration of the parameter (instead of its free aqueous form) and the subscript $_{(cc)}$ refers to the concentrations in the calcite. Data is marked by black circles from the [DIC] experiment, red triangles from the $[Ca^{2+}]$ experiment, yellow filled diamonds from the $[DIC] - [Ca^{2+}]$ experiment and blue filled squares from the $pH - [Ca^{2+}]$ experiment. Datapoints from experiments are not shown in the subfigure when the plotted parameter was kept constant during the experiment. Error bars of the $EI/Ca_{(cc)}$ represent $\pm 2\sigma$ standard deviation, when no error bar is plotted, the error is smaller than the symbol used.

considered here significant.

2.5. Raman spectroscopy and Scanning Electron Microscopy

Raman spectroscopic analysis was used to confirm the mineral phase of each of the precipitated overgrowth samples. Surface measurements were conducted using the Kaiser Optical Systems micro-Raman instrument at the Hawai'i Institute of Geophysics and Planetology in accordance with the procedures described in Conner et al. (2023). A 785 nm red laser was used as the excitation source. GRAMS/AI software (Thermo Fisher Scientific Inc.) was used to calculate the peak positions representing internal (ν_1 , ν_4 peaks) and lattice (L and T peaks) vibrational modes, which vary among different calcium carbonate phases like calcite or aragonite.

Images of the calcite surface morphology were obtained by Scanning Electron Microscope (SEM, Hitachi TM3000) at the NIOZ. The low vacuum mode used in this device provides tolerance against moisture and charge, which allows the observation of samples without coating.

Uncoated samples, mounted on the adhesive surface of the SEM stubs, were analyzed at an accelerating voltage of 15 kV and the images were generated in the standard SEM software (TM3000).

3. Results

3.1. El/Ca ratios in calcite

In the experimental solutions under various carbon chemistry conditions, the S/Ca_(cc) values ranged from 26.8 to 36.9 mmol mol⁻¹, Mg/Ca_(cc) values between 1.9 and 6.1 mmol mol⁻¹, B/Ca_(cc) values between 340 and 486 µmol mol⁻¹, and Na/Ca_(cc) varied between 1.7 and 2.2 mmol mol⁻¹. While [SO $_4^2$]_(total), [Mg 2 +]_(total), and [B]_(total) remained the same for all experiments, [Na+] did change across our experiments, depending on the targeted solution [DIC] levels (as Na₂CO₃ was used as the DIC source: Section 2.1). Because the main focus of this work is on Sincorporation, our Mg/Ca_(cc), B/Ca_(cc), and Na/Ca_(cc) data are briefly discussed in the Supplementary Information (SI 1, Supplementary

Table 2 R^2 and p-values calculated based on linear regressions between S/Ca_(cc) ratios and [DIC], [CO $_3^2$]_(total), [HCO $_3$]_(total), pH_{NBS}, [Ca 2 +]_(total), calcite saturation state (Ω), precipitation rate, Mg/Ca_(cc), B/Ca_(cc), Na/Ca_(cc) as plotted on Fig. 2. R^2 and p-values are not shown when the parameter was kept constant.

	[DIC] exp.		[Ca ²⁺] exp.		$[DIC] - [Ca^{2+}] exp.$		pH – [Ca ²⁺] exp.	
	R^2	p-value	R^2	p-value	R^2	p-value	R^2	<i>p</i> -value
[DIC]	0.87	0.00	_	_	0.92	0.00	_	_
$[CO_3^{2-}]_{(total)}$	0.87	0.00	0.96	0.00	0.85	0.00	0.90	0.00
[HCO ₃] _(total)	0.87	0.00	0.96	0.00	0.93	0.00	0.95	0.00
pH_{NBS}	_	_	_	_	_	_	0.98	0.00
[Ca ²⁺] _(total)	_	_	0.96	0.00	0.94	0.00	0.95	0.00
Calcite saturation state	0.87	0.00	0.96	0.00	_	_	_	_
Precipitation rate	0.82	0.00	0.92	0.00	_	_	_	_
Mg/Ca _(cc)	0.53	0.01	0.93	0.00	0.87	0.00	0.94	0.00
B/Ca _(cc)	0.06	0.46	0.99	0.00	0.92	0.00	0.59	0.00
Na/Ca _(cc)	0.46	0.01	0.63	0.01	0.10	0.32	0.92	0.00

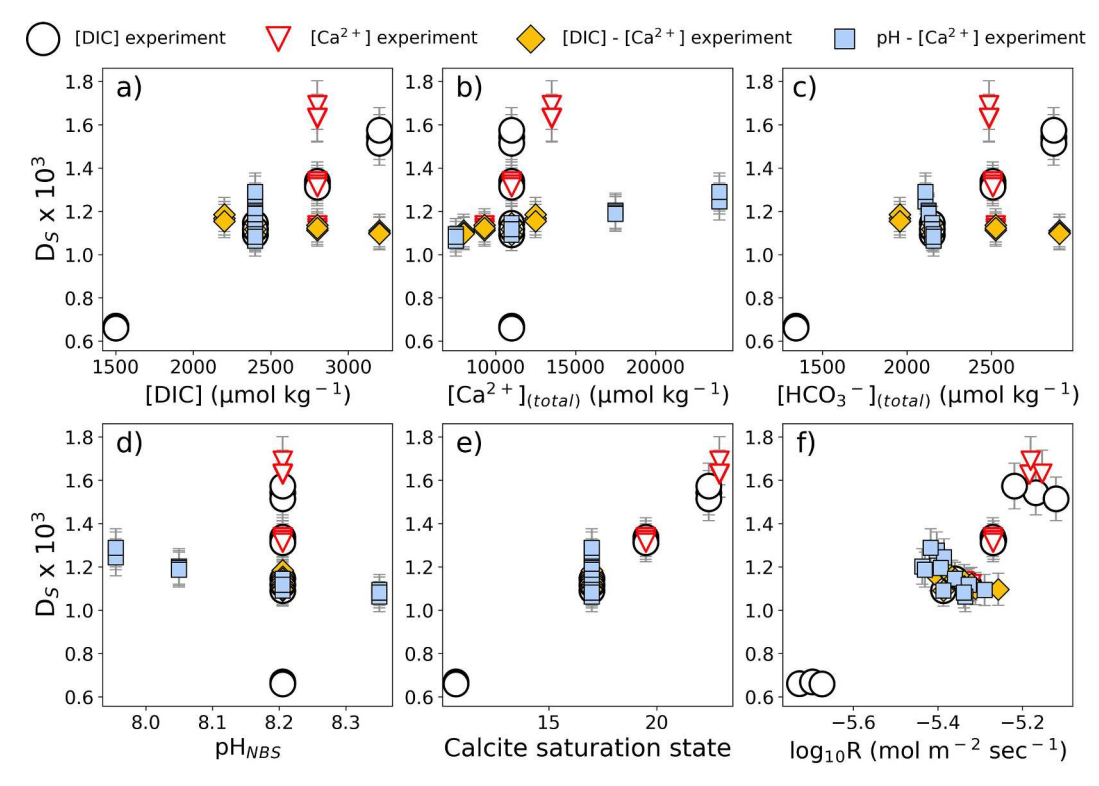


Fig. 3. Sulfur partition coefficient (D_s) expressed with $[CO_3^2]_{(total)}$ in the denominator is plotted against a) [DIC], b) $[Ca^{2+}]_{(total)}$, c) $[HCO_3^-]_{(total)}$, d) pH_{NBS} , e) calcite saturation state (Ω) , and f) precipitation rate. Data is marked by black circles from the [DIC] experiment, red triangles from the $[Ca^{2+}]$ experiment, yellow filled diamonds from the $[DIC] - [Ca^{2+}]$ experiment and blue filled squares from the $pH - [Ca^{2+}]$ experiment. Error bars of the D_s values represent propagated error based on $\pm 1\sigma$ standard deviation of the measured $S/Ca_{(cc)}$ values, the carbon system calculations using Monte Carlo simulations, and the uncertainty from the preparation of the growth solution (i.e., weighing of chemicals).

Figure S2, Figure S3, Figure S4).

The largest spread in $S/Ca_{(cc)}$ values (i.e. the difference between the lowest and highest sulfate abundance in the calcite samples) were found in the pH - [Ca²+] experiments. During this set of experiments, both pH and [Ca²+]_(total) were concurrently varied to keep Ω constant, for direct characterization of the effect of pH on sulfate incorporation without kinetic biases. We observed a significant negative linear correlation between $S/Ca_{(cc)}$ ratios of the calcite with pH (Fig. 2 d, Table 2). At the same time, because the decrease of 0.395 pH_{NBS} unit was compensated with an increase of 16.5 mM [Ca²+]_(total), a positive trend, best described as a logarithmic relation, could be observed between $S/Ca_{(cc)}$ and [Ca²+]_(total) (Fig. 2 e).

Experimental conditions within the [DIC] series also had variations in [DIC], $[CO_3^2]_{(total)}$ and $[HCO_3^2]_{(total)}$, while $[Ca^{2+}]_{(total)}$ and pH were constant. The strong impact of the carbonate system on $S/Ca_{(cc)}$ within this series could be observed by a positive correlation with [DIC], $[CO_3^2]_{(total)}$, $[HCO_3^2]_{(total)}$, and Ω (Fig. 2 a-c, f). As Ω and R correlated linearly in this experiment, an increase of $S/Ca_{(cc)}$ with R was equally apparent.

In the [Ca²⁺] experiment, both [DIC] and pH were kept constant. An increase of 4.2 mM [Ca²⁺]_(total) from the low to high [Ca²⁺]_(total) conditions of this set of experiments resulted in a 35 % increase in Ω . The incorporation of sulfate correlated positively with [Ca²⁺]_(total) and thus also with Ω and R (Fig. 2 e-g). Variation in [CO $_3^2$ -]_(total) was smaller within this experiment compared to those in which [DIC] varied, but S/ Ca_(cc) still increased with higher [CO $_3^2$ -]_(total) values.

The [DIC] - [Ca²⁺] experiments aimed to investigate the impact of carbon chemistry at a constant Ω and R. The addition of [DIC] was hence compensated with decreasing [Ca²⁺]_(total). In this case, sulfate incorporation decreased at higher [DIC] and [HCO $_3$]_(total), as opposed to the pattern observed in the [DIC] experiments (Fig. 2 a, c). Sulfate incorporation in the [DIC] - [Ca²⁺] experiments showed a clear positive

dependence to an increase in $[Ca^{2+}]_{(total)}$, as observed also in the $[Ca^{2+}]$ and pH - $[Ca^{2+}]$ experiments (Fig. 2 e).

Sulfate incorporation showed diverse trends when compared to the other elements analyzed in this study. A significant negative linear correlation was shown between $S/Ca_{(cc)}$ and $Mg/Ca_{(cc)}$ values of the calcite (Fig. 2 h, Table 2). Similarly, a negative trend was observed between $S/Ca_{(cc)}$ and $B/Ca_{(cc)}$ within the pH-[Ca²⁺] experiments, but a positive relationship was seen between $S/Ca_{(cc)}$ and $B/Ca_{(cc)}$ in the [DIC]-[Ca²⁺] and [Ca²⁺] experiments (Fig. 2 i). The $S/Ca_{(cc)}$ ratios generally correlated positively with Na/Ca_(cc) in the [DIC], [Ca²⁺] and pH-[Ca²⁺] experiments, although sensitivities to changes in Na/Ca_(cc) varied extensively within each experiment series (Fig. 2 j).

3.2. Sulfate partitioning in calcite

Partitioning of elements between the dissolved and the solid phase can be expressed as $D_{El} = ([El]/[Ca])_{solid} / ([El]/[Ca])_{fluid}$, when substitution of the element occurs at the expense of Ca²⁺ in the crystal lattice. Sulfate ions, however, substitute for CO₃² (Pingitore et al., 1995) so that its partitioning in CaCO3 should be expressed with respect to $[CO_3^{2-}]$. As the stoichiometry between calcium and carbonate equals one in the crystal structure, we defined the sulfur partition coefficient as D_s $=([SO_4^{2-}]/[CO_3^{2-}])_{calcite}/([SO_4^{2-}]/[CO_3^{2-}])_{solution}$, where we assumed $([SO_4^{2-}] / [CO_3^{2-}])_{calcite}$ can be approximated by our measured S/Ca_(cc) values. The D_s values responded positively and linearly to changes in precipitation rate (p < 0.0000001; R² = 0.71) and Ω (p < 0.0000001; R² = 0.92; Fig. 3). As R and Ω are coupled and covaried linearly within these experiments, isolating potentially independent effects was not possible within this study. R correlated with Ω slightly less than how D_s correlated with Ω , which is due to uncertainties in the estimation of R while Ω was one of the pre-determined parameters of this study.

 D_s also correlated with pH in our pH - [Ca²⁺] experiment (p <

Fig. 4. SEM images of a) calcite seeds used for nucleating calcite precipitation and b) calcite samples from the [DIC] experiment – Condition C and c) the pH – [Ca²⁺] experiment – Condition C as described in Table 1 shown as examples for the calcite surface morphology.

0.000001; $R^2=0.93$; Fig. 3 d). Although we observed a dependence of D_s to pH, there was a large range in D_s values in all other experiments in which pH was kept constant. Variation in seawater pH inherently also affected $[CO_3^{2-}]$ and thus influenced Ω and precipitation rate. Within the pH - $[Ca^{2+}]$ experiments, $[Ca^{2+}]_{(total)}$ was additionally varied in order to keep the Ω constant and thus isolate the effect of precipitation rate from that of pH. In this case, values of D_s decreased with increasing pH, suggesting additional controls on sulfate partitioning beyond the influence of the Ω and R. As both pH and $[Ca^{2+}]_{(total)}$ were varied here, further experiments would be required to fully decouple the effect of these two parameters.

3.3. Raman spectroscopy and Scanning Electron Microscopy

Raman spectra of all samples showed the characteristic peak positions for calcite (Supplementary Figures S5 and S6), as well as one additional – albeit very weak – peak at about 1017 cm⁻¹ that was not indicative of calcite. No significant variation in calcite surface morphology was observed in relation to the changing solution chemistry (Fig. 4). The well-defined sharp edges of the rhombohedral calcite seeds, however, could not be recognized on the calcite overgrowth. The calcite crystals were characterized by roughened and angled edges, showing new faces developing on the corners.

4. Discussion

4.1. CaCO₃ mineralogy and precipitation pathways

All polymorphs of CaCO₃ have the capacity to incorporate sulfate but to what extent varies with the density of the CaCO3 structure (Arroyo-de Dompablo et al., 2015; Midgley et al., 2020). The incorporation of the tetrahedral configuration of sulfate into CaCO₃ is more stable in calcite, than in the denser aragonite crystal structure (Arroyo-de Dompablo et al., 2015; Midgley et al., 2020). The presence of sulfur (and often in combination with Mg2+ in solutions) will generally enhance the formation of aragonite (Bots et al., 2011; Tang et al., 2012) and vaterite (Fernández-Díaz et al., 2010; Grasby, 2003). However, [SO₄²⁻]_(total) and [Mg²⁺]_(total) of our experimental solutions were apparently too low to induce the precipitation of non-calcite polymorphs (Bots et al., 2011), since we find no trace of aragonite and vaterite in the CaCO3 samples generated in our experiments based on Raman spectroscopy (Supplementary Figure S5). Additionally to the characteristic vibrational mode peaks of calcite, Raman spectra of our samples display a weak band at 1017 cm⁻¹. Note that this band aligns with the symmetric S-O stretching mode (i.e., the v_1 peak) of type-II – or insoluble – anhydrite (Prieto-Taboada et al., 2014; Schmid et al., 2020). However, we argue that this peak does not point to the presence of anhydrite with calcite in our samples because direct precipitation of anhydrite is extremely unlikely in our low-temperature aqueous experiments without any significant aging of the mineral-solution mixture (Ossorio et al., 2014). As all precipitating solutions of these experiments were undersaturated with

respect to anhydrite and gypsum, the peak present close to the typical position of the Ca-SO₄ phases in the spectrum (Prieto-Taboada et al., 2014; Schmid et al., 2020) indicates the incorporation of sulfate in the calcite structure, rather than CaSO₄ being precipitated. Also, no crystal phase other than CaCO₃ could be identified during the SEM analysis. Surface morphological transformation from the sharp edges of the calcite seeds to the roughened edges of the grown calcite is consistent with Uchikawa et al. (2023), who performed calcite precipitation experiments using the same approach in SO_4^{2-} -bearing solutions (see Fig. 1 therein).

Under certain conditions, inorganic CaCO₃ experiments could result in formation of amorphous CaCO3 (ACC), which can rapidly transform into calcite (e.g., Blue et al., 2017; Radha et al., 2010). Presence of SO₄² and Mg²⁺ ions in the solution have profound impacts on the formation and stability of ACC, as well as on the polymorph formed after the transformation (Blue and Dove, 2015; Goetschl et al., 2021; Konrad et al., 2018). Incorporation of major and trace elements as a function of changes in solution carbon chemistry parameters, such as pH, likely follow similar patterns in inorganic calcite and ACC (Evans et al., 2020), but composition of the crystalline CaCO3 polymorph formed from a precursor phase depends on the transformation pathways. Hence, whether our calcite samples were formed directly or indirectly via ACC, has implications on how to interpret our S/Ca_(cc) and D_s data. While solid state transformation is likely to conserve much of the initial elemental and isotopic signature of sulfate (e.g., Walker et al., 2017), dissolution-recrystallization may increase or decrease calcite S/Ca values depending on the sulfate concentration of the ambient solution (e.g., Nielsen et al., 2014). The presence of ACC in CaCO3 samples is easily identifiable by Raman spectroscopy for the lack of lattice mode peaks compared to crystalline CaCO3 polymorphs (Supplementary Figure S6 modified after DeCarlo, 2018). However, phase transformation of ACC to more stable crystalline CaCO3 is known to occur even in air, provided some moisture is present (Konrad et al., 2016), and hence, the potential ACC signal could dissipate over time during sample storage. By noting this issue, we used a sub-sample from the baseline condition of our CaCO₃ precipitation experiments to perform immediate Raman analysis at 15 random spots within one hour after collection. Results show no evidence of ACC, and calcite is the only identifiable CaCO₃ phase.

Although the presence and short-term transformation of ACC cannot be completely ruled out, conditions in our experiments (e.g., low degrees of supersaturation and low solution Mg/Ca ratio) are more likely to promote direct precipitation (Giuffre et al., 2015). We echo that our experimental solutions had $[\mathrm{SO}_4^{2-}]_{(total)}$ and $[\mathrm{Mg}^{2+}]_{(total)}$ apparently too low to promote the precipitation of aragonite and vaterite over calcite, whereas templated CaCO $_3$ precipitation enabled by the calcite seeds also aids continuous and exclusive calcite precipitation (Mucci et al., 1989; Romanek et al., 1992; Zeebe and Sanyal, 2002). Consequently, our S/Ca and D $_8$ data should reflect sulfate incorporation explicitly for calcite without any bias caused by other polymorphs or ACC.

4.2. Potential relationships between different El/Ca ratios

The S/Ca_(cc) values analyzed in the calcite samples grown in our experiments show remarkably high values when compared to those produced by Busenberg and Plummer (1985) at higher solution $[SO_4^{2-}]_{(total)}$ (approximately 20 mM difference). Although $[Ca^{2+}]_{total}$ of the experimental solutions are within the same range (7.5–24 mM), solution pH_{NBS} values were at least 0.58 unit lower in Busenberg and Plummer (1985). If the experimental data from the two studies are compared in D_s values to account for differences in solution chemistry (i. e., $[SO_4^{2-}]_{(total)}$ and $[CO_3^{2-}]_{(total)}),$ the D_s values recalculated for Busenberg and Plummer (1985; $0.1 \times 10^3 - 0.9 \times 10^3$ at Ω : 2-15) are consistent with the values presented here, except for the D_s obtained for the highest Ω (1.1 × 10³ at Ω = 30) which is lower than expected based on our results. Uchikawa et al. (2023) grew calcite in solutions of CaCl₂ – $Na_2CO_3 - B(OH)_3 - Na_2SO_4$ where the addition of $[SO_4^{2-}]_{(total)} = 5$ mM and $[Ca^{2+}]_{(total)} = 5.4$ mM contributed to similar S/Ca_(cc) (28.7 mmol mol $^{-1}$) and D_s (0.4 \times 10 3 at $\Omega=9.3$) values as within this study. Wynn et al. (2018) conducted inorganic experiments at significantly lower $[SO_4^{2-}]_{(total)}$ (20.8 μM and 208.2 μM) and Ω (<12) and reported D_s values $(0.05 \times 10^3 - 1.08 \times 10^3)$ that are generally comparable to the values obtained in our experiments. While they show the equivalent pH dependence on the overall sulfate incorporation with a negative relationship between S/Ca_(cc) and pH as within this study (Fig. 2 d), the D_s values of Wynn et al. (2018) increase with increasing pH, suggesting multiple controls on sulfate substitution.

An important consideration for data comparison across these independent studies is the differences in solution chemistry compositions, for instance the presence or absence of Mg²⁺ and boron, that could potentially modulate the incorporation of multiple elements via cooperative incorporation. Absorption spectroscopy (Pingitore et al., 1995; Takano, 1985; Takano et al., 1980) and other lines of crystallographic evidence (Fernández-Díaz et al., 2010; Kontrec et al., 2004; Okumura et al., 2018) indicate that the tetrahedral SO₄²⁻ is substituting for trigonal planar CO_3^{2-} , causing significant structural changes in the calcite lattice. Considering the lattice distortion caused by the stretched apical oxygen of the SO_4^{2-} anion, it has been suggested that incorporation of sulfate often occurs in close associations with other cations (Okumura and Kitano, 1986; Takano, 1985) or anions (Uchikawa et al., 2023). Cations with a smaller ionic radius than Ca^{2+} , such as Mg^{2+} and Na^+ present in our experimental solutions can cause a contraction in the calcite cell unit (Busenberg and Plummer, 1985; Paquette and Reeder, 1990; Takano, 1985) and thereby potentially counter-balance the calcite lattice distortions caused by SO₄²⁻ (Kontrec et al., 2004). Studies on element incorporations in biogenic carbonates reported a strong positive covariance between these cations and sulfate (Grossman et al., 1996; Lorens and Bender, 1980; Van Dijk et al., 2019a), supporting a cooperative incorporation mode. Although the data presented here also show a co-variance between incorporated sulfate and magnesium (Fig. 2 h), as also revealed in Goetschl et al. (2019), the trend is negative and hence not in line with the observations for biogenic carbonates. This implies that it is unlikely that magnesium as such is an enhancing factor for the incorporation of SO_4^{2-} . Similarly, the lack of unifying trend between Na/ $Ca_{(cc)}$ and $S/Ca_{(cc)}$ under the conditions of the four experimental series (Fig. 2 j) makes a mechanistic coupling between sodium- and sulfate incorporation unlikely. Sodium and sulfate partitioning are hence more likely linked indirectly, for instance via changes in growth rate (Devriendt et al., 2021), as also indicated for sulfate (Fig. 3 e, f) and sodium (Supplementary Figure S4) in the current study.

Uchikawa et al. (2023) also proposed a possible crystallographic link between sulfate and boron incorporation on the basis of lattice distortion and supposedly structural support in the calcite lattice. If the enhanced sulfate adsorption reduces the physical barrier for boron incorporation (or vice versa), one would expect a linear increase of $S/Ca_{(cc)}$ with increasing $B/Ca_{(cc)}$. However, such relation is not clearly reflected in the results of this study (Fig. 2 i). For instance, for the pH –

[Ca²⁺] experiments, where both pH and [Ca²⁺]_(total) are varied, S/Ca_(cc) is negatively correlated to B/Ca_(cc). While these observations do not rule out the possibility of cooperative incorporation, the final patterns for these different ions are likely overwritten by other controls, such as changes in inorganic carbon chemistry and CaCO₃ precipitation kinetics.

4.3. Dependence on calcite precipitation kinetics

The rate at which CaCO3 precipitates significantly influences the incorporation of minor and trace elements. In our [DIC], and [Ca²⁺] experiments, both S/Ca_(cc) (Fig. 2 g) and D_s values (Fig. 3 f) show a pronounced increase with an increase in R. These trends are consistent with the results reported by Busenberg and Plummer (1985), suggesting kinetic controls on sulfate incorporation. It is commonly thought that higher Ω increases the defect site density on the calcite surface. Rapid precipitation induces more structural defects, being present as unoccupied kinks (Busenberg and Plummer, 1985; Teng et al., 2000). Since the ion binding potential is likely higher at these defect sites due to the incomplete bonding environment (Larsen et al., 2010), sulfate incorporation associated with the structural defects could partly explain the impact of R on D_c observed here. Moreover, precipitation rate will likely impact attachment and detachment rates of sulfate from the calcite surface (DePaolo, 2011). At slow precipitation rates, any adsorbed sulfate has higher potential to desorb from the surface, while higher precipitation rates will result in a more likely incorporation of adsorbed

However, the pH - [Ca $^{2+}$] and DIC - [Ca $^{2+}$] series were conducted at constant Ω , and therefore we observe hardly any difference in R across all experiments. Yet, S/Ca $_{(cc)}$ ratios and D $_s$ values show notable trends as a function of changes in certain carbon system parameters. For example, in the pH - [Ca $^{2+}$] series, a negative linear dependence to pH is evident for both S/Ca $_{(cc)}$ and D $_s$ (Fig. 2 d and 3 d). Since R does not change in these experiments, the observed S/Ca $_{(cc)}$ and D $_s$ variations as a function of pH within this series cannot be explained by kinetic effects and suggest additional factors that influence sulfate incorporation.

4.4. Mechanistic link between sulfate incorporation and pH

Results of this study suggest that sulfate partitioning in calcite has an inverse dependence on pH changes of the growth solution, when the impact of pH on R are effectively compensated by concurrent [Ca²⁺]_(total) adjustment (Fig. 2 d and 3 d). Exchange of cations and anions at the calcite surface is essentially controlled by differences in charge balance and the alterations in (and fit within) the calcite crystal structure. The isoelectric state pH, at which the calcite surface is electrically neutral, has been defined to be close to pH_{NBS} 8.2 (Siffert and Fimbel, 1984; Somasundaran and Agar, 1967) although it can be affected by adsorption of ions including excess Ca²⁺ (e.g., Cicerone et al., 1992; Wolthers et al., 2008). When calcite is growing in solutions with pH_{NRS} above \sim 8.2, cations will be attracted to the calcite surface, while the calcite surface will become positively charged and anion attachment will be enhanced in solution with pH $_{NBS}$ less than ${\sim}8.2$ (Amankonah and Somasundaran, 1985; Siffert and Fimbel, 1984; Somasundaran and Agar, 1967). Three of the four experimental series of this study were performed at $pH_{NBS}=8.205\pm0.03,$ that is close to the zero point of charge, while our pH - [Ca²⁺] experiment comprises a range of pH_{NBS} conditions between 7.995 and 8.350. Although we do not expect significant change in charge balance within such a small range of pH (Foxall et al., 1979; Somasundaran and Agar, 1967), we still observe increased sulfate incorporation at lower pH than at higher pH in the pH - [Ca2+] experimental series. This could be due partly to some differences in charge balance at the calcite surface.

The potential pH effect on sulfate incorporation may explain the relationship between the $S/Ca_{(cc)}$ values and seawater $[CO_3^2]_{(total)}$ observed for foraminiferal CaCO₃. Van Dijk et al. (2017) studied the effect of $[CO_3^2]_{(total)}$ and reported that the foraminifera incorporate

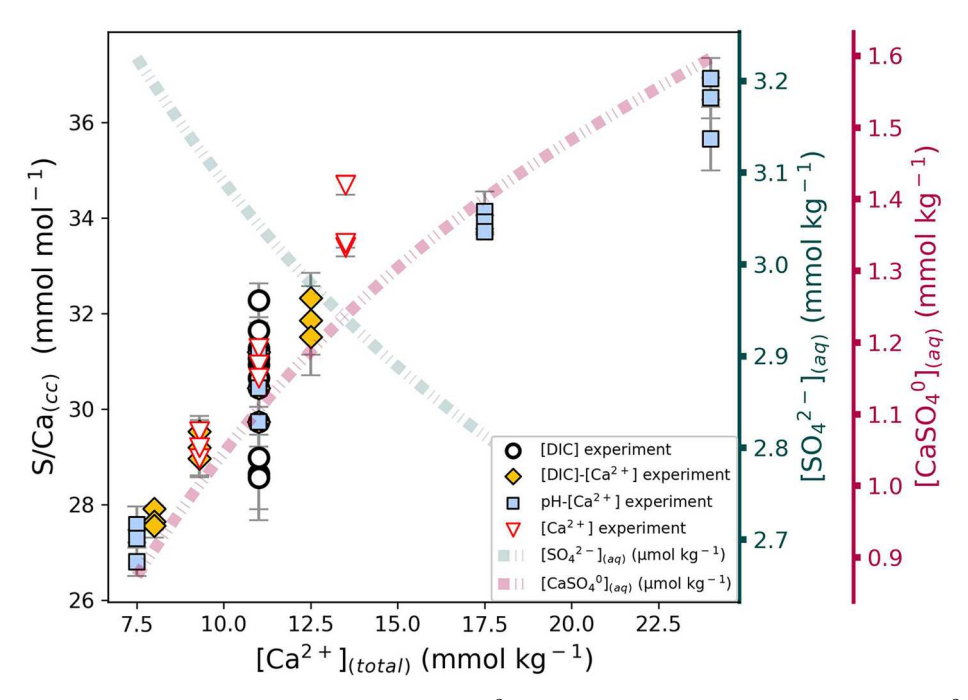


Fig. 5. Calcite $S/Ca_{(cc)}$ values (black circles: [DIC] experiment, red triangles: $[Ca^{2+}]$ experiment, yellow filled diamonds: $[DIC] - [Ca^{2+}]$ experiment, blue filled squares: $pH - [Ca^{2+}]$ experiment), free aqueous SO_4^{2-} concentrations (green dash dotted line) and aqueous $CaSO_4^0$ concentrations (pink dash dotted line) plotted against total concentrations of Ca^{2+} in the solution. The plot shows the positive correlation between $S/Ca_{(cc)}$ values and $[CaSO_4^0]_{(aq)}$. Error bars represent $\pm 2\sigma$ standard deviation of the duplicate measurement.

more sulfate when $[CO_3^2]$ of the ambient seawater is lower. However, changes to the carbon system parameters were applied by the addition of CO_2 , which consequently involved changes in both $[CO_3^2]_{(total)}$ and pH in their culturing experiments. As these parameters were coupled, an increase of $129\,\mu\text{mol}\,k\text{g}^{-1}$ in $[CO_3^2]_{(total)}$ involved simultaneous changes in pH_{NBS} between 7.6 and 8.1 (i.e., lower $[CO_3^2]_{(total)}$ coincided with lower seawater pH). Thus the proposed effect of $[CO_3^2]_{(total)}$ on sulfate partitioning in foraminifera could indirectly be caused by variation of pH in these experiments.

Alternatively, decreasing S/Ca_(cc) values with increasing pH could be explained by changes in the ratio of free aqueous SO_4^{2-} anion to CO_3^{2-} (Busenberg and Plummer, 1985). Previous inorganic CaCO₃ experiments indicated that the activity ratio of the respective ions (aSO_4^{2-}/aCO_3^{2-}) impacts sulfate incorporation both in calcite and aragonite (Busenberg and Plummer, 1985; Fernández-Díaz et al., 2010) and this influence is more prominent than the effect of precipitation rate (Barkan et al., 2020). This is in line with Frisia et al. (2005), suggesting that the variability in sulfate concentrations in stalagmites may result from seasonally changing pH of seepage water, which modulates the HCO $_3^{2-}$ and CO_3^{2-} speciation and thus the $[SO_4^{2-}]_{(total)}$ / $[CO_3^{2-}]_{(total)}$ ratio.

A positive correlation between $S/Ca_{(cc)}$ and aSO_4^2-/aCO_3^2 is also evident in our data, but only for those experiments where R is kept constant (i.e., $[DIC] - [Ca^{2+}]$ and $pH - [Ca^{2+}]$ experiments; Supplementary Figure S7). Moreover, note that variations in pH will not only affect total concentrations of CO_3^{2-} in solution but also the species distribution of other anions and cations (Byrne, 2003). Substantial occupation of aqueous SO_4^{2-} or other cations that may form complexes with SO_4^{2-} can potentially limit the availability of the preferred sulfate species for incorporation in the calcite.

4.5. Calcite incorporation of sulfate via $CaSO_4^0$ ion-pairs

While our data indicate some degree of $S/Ca_{(cc)}$ sensitivity to changes in pH, and hence $[CO_3^2]_{(total)}$ and the solution $[SO_4^2/CO_3^2]$ ratio, contrasting patterns of $S/Ca_{(cc)}$ versus $[CO_3^2]_{(total)}$ as shown in Fig. 2 b, suggest that a large part of the variability in our $S/Ca_{(cc)}$ can be

explained by the differences in R (i.e., kinetic effects) and/or solution chemistry (i.e., distribution of free and complexed ionic species).

The largest proportion of the total dissolved sulfate in seawater exists as free sulfate ion, but a significant amount of sulfate also forms ion pairs, such as CaSO₄, MgSO₄, KSO₄, and NaSO₄ (Byrne, 2003; Garrels and Thompson, 1962). Under our experimental conditions, 59-72 % of the total sulfate concentration of the solution is present in the form of free SO_4^{2-} anions, while there are notable variations in sulfate speciation between SO_4^{2-} and $CaSO_4^{0}$ across the pH – [Ca²⁺] experiments (Table 1). The largest impact on sulfate speciation is caused by the change in [Ca²⁺]_(total). As the total sulfate concentration is kept constant in all experiments, the increase in [Ca²⁺]_(total) corresponds with the increase of $[CaSO_4^0]_{(aq)}$ and concurrent decrease of $[SO_4^{2-}]_{(aq)}$ (Fig. 5). If the free sulfate anion is indeed the main species incorporated into calcite (Pingitore et al., 1995; Takano, 1985; Takano et al., 1980), one would expect an increase in calcite S/Ca(cc) values with an increase in $[SO_4^{2-}]_{(aq)}$ or a decrease in $[Ca^{2+}]_{(aq)}$. Instead, we observe the opposite pattern - a linear negative correlation (Fig. 5 and Supplementary Figure S8 a) – suggesting that SO_4^{2-} is not the primary promoter for sulfate incorporation in our experiments. Among all dissolved complexes formed by sulfate under the experimental conditions of this study, only $[CaSO_4^0]_{(aq)}$ correlates positively with calcite S/Ca_(cc) values (Fig. 5, also see Supplementary Figure S8). Though aqueous CaSO₄ comprises only 19-35 % of the total sulfate concentration, it might provide an appreciable contribution to S incorporation and hence S/Ca values of the

Only one series of experimental conditions, the [DIC] experiment, keeps $[\text{Ca}^{2+}]_{(\text{total})}$ constant, while the other three experiment series cover a range of 7.5 to 24 mM $[\text{Ca}^{2+}]_{(\text{total})}$. Calculations of the distribution of sulfate species reveal a 1 % increase of the $[\text{CaSO}_4^0]_{(\text{aq})}$ per 1 mmol kg $^{-1}$ increase in solution $[\text{Ca}^{2+}]_{(\text{total})}$ (Table 1). As the pH increase (during the pH - $[\text{Ca}^{2+}]$ experiment) does not contribute to any further change in $[\text{CaSO}_4^0]_{(\text{aq})}$ beyond the 1 % increase caused by the change in $[\text{Ca}^{2+}]_{\text{total}}$, one may suspect that $[\text{Ca}^{2+}]_{(\text{total})}$ of the solution could impose the same, or potentially even larger, impact on sulfate partitioning than pH. Elevated $[\text{Ca}^{2+}]_{(\text{total})}$ contributes to the complexation of

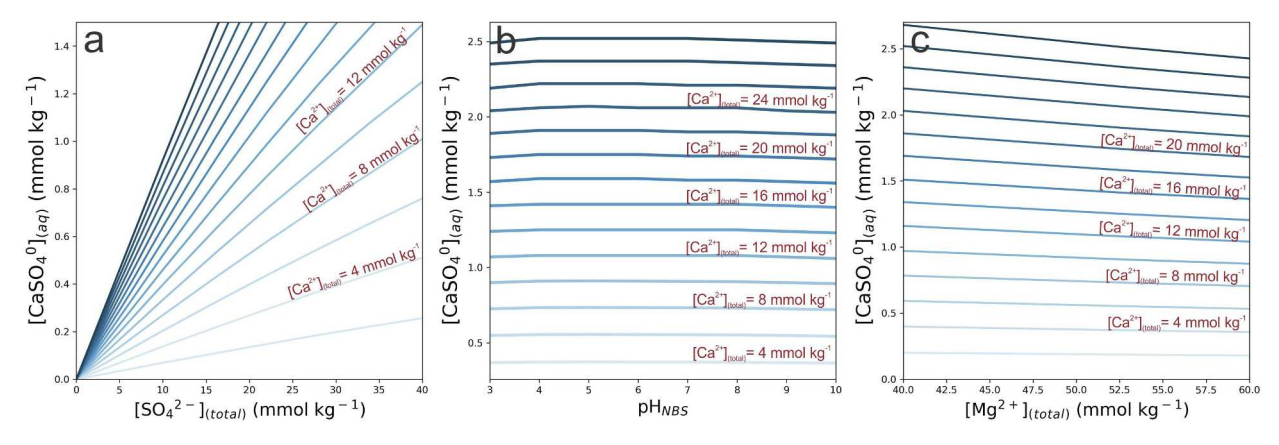


Fig. 6. $CaSO_4^0$ complex formation calculated using the PHREEQC solution chemistry model (Version 3; Parkhurst and Appelo, 1999) for constant $[B(OH)_4 + B(OH)_3]$ (0.420 mmol kg^{-1}), [DIC] (2.40 mmol kg^{-1}), [Cl $^-$] (550 mmol kg^{-1}) and various $[Ca^{2+}]_{(total)}$ plotted against a) $[SO_4^{2-}]_{(total)}$, b) pH_{NBS} , and c) $[Mg^{2+}]_{(total)}$ (SO $_4^{2-}]_{(total)}$ on plot a) and c), and $[Mg^{2+}]_{(total)}$ on plot a) and b) are 28.2 mmol kg^{-1} and 52.8 mmol kg^{-1} , respectively. Light blue lines indicates lower $[Ca^{2+}]_{(total)}$ and dark blue lines show high $[Ca^{2+}]_{(total)}$.

a larger proportion of the solution's sulfate content, enhancing sulfate incorporation by providing a higher concentration of the CaSO₄ ion pair.

Note that incorporation of sulfate as CaSO₄ complex should result in the same structural deformation as the substitution with a single anion of sulfate for CO₃²⁻ (Fernández-Díaz et al., 2010). However, due to the difference in the charge and structure of the hydration sphere, CaSO₄ is expected to undergo quite different surface adsorption, desolvation, and incorporation processes than the free SO₄²⁻. For example, solution energies reported by Midgley et al. (2020) suggest that the adsorption of sulfate on the calcite surface in the form of a Ca-sulfate complex is energetically more favorable than the adsorption of a single sulfate anion. But the actual physical processes by which ion-pairs, such as CaSO₄, are incorporated into CaCO₃ minerals and how those would compare to a case where elemental uptake occurs via free uncomplexed ions are significantly understudied and poorly characterized. Preferential adsorption and/or incorporation of ion complexes over free ions has previously been shown for only divalent cations. A large fraction of Mn²⁺ and Mg²⁺ attach on the calcite surface as an ion-pair formed with CO₃²⁻ (Mills et al., 2022). Incorporation of Mn²⁺ and Mg²⁺ as ion-pairs with CO_3^{2-} potentially also explains their calcite inhibiting behavior. While dehydration of these cations through complex formation aids a more accessible attachment on the calcite surface, this likely limits CO_3^2 reorientations at the kink sites (Mills et al., 2022). Sulfate has been suggested to promote desolvation of cations (e.g., Piana et al., 2006; Yang et al., 2012), and hence complex formation of SO₄²⁻ and Ca²⁺ helps dehydration of Ca²⁺ that is generally considered the rate determining step for calcite growth (Wolthers et al., 2012 and references therein). CaSO₄ ion pair effectively results in sulfate substituting for carbonate in the calcite crystal structure and therefore CaSO₄ ion pair adsorption and incorporation is a mechanistic explanation for previous observations of

We additionally acknowledge that Mg^{2+} readily forms complexes also with SO_4^{2-} (and not only with CO_3^2 as described above) to form $MgSO_4^0$ (Garrels and Thompson, 1962), which could be favored over SO_4^{2-} incorporation into the calcite lattice (Sakuma et al., 2014). The results of this study do not indicate a significant contribution of $MgSO_4^0$ to the sulfate incorporation (Supplementary Figure S8 c), but it still might provide a major contribution to the Mg^{2+} content of the calcite (Kralj et al., 2004). Interestingly, the relation between $S/Ca_{(cc)}$ and $[MgSO_4^0]_{(aq)}$ may vary under different temperature conditions because magnesium incorporation is well-known to increase with increasing temperature (e.g., Lea et al., 1999; Mejri et al., 2014). The distribution of sulfate species is independent of temperature, but the preferred form of incorporated sulfate complex could potentially be (indirectly) affected by the temperature control on Mg^{2+} incorporation and thus the sulfate

incorporation via MgSO $_4^0$ may be preferred over CaSO $_4^0$. Exploring this possibility requires further work as all experiments here were performed at a constant temperature (23 \pm 0.3 °C). Also, the current Mg/Ca ratio of seawater is approximately 5 mol/mol, while the simplified and dilute solutions of these experiments contained a Mg/Ca ratio < 0.3 mol/mol. If [Mg $^{2+}$](total) was higher relative to [Ca $^{2+}$](total) in our experimental solutions, free sulfate anions have a larger potential to form complexes with Mg $^{2+}$ over Ca $^{2+}$. It follows that MgSO $_4^0$ could play a more important role for S incorporation, for example in seawater, than what is observed in our experiments.

4.6. Sensitivity of D_s for past changes in seawater sulfate and calcium concentrations

Sections 4.3 and 4.4 discussed the potential dependence of sulfate incorporation on Ω and pH with the assumption that sulfate is incorporated into CaCO₃ as the free SO₄²⁻ anion (Pingitore et al., 1995; Takano, 1985; Takano et al., 1980). However, as we addressed in Section 4.5., the results from this study suggest that free aqueous SO_4^{2-} may not be the (only) form of sulfate taken up, and instead, complexed forms of sulfate also contribute to sulfur incorporation. Specifically, we argue that the availability of CaSO₄⁰ (or MgSO₄⁰) complexes will at least partly affect the S/Ca_(cc) values in inorganic calcites. The abundance of CaSO₄ ion pairs ultimately depends on [SO₄²⁻]_(total) and [Ca²⁺]_(total). Computations by PHREEQC (Version 3; Parkhurst and Appelo, 1999) reveal that 1 mmol kg^{-1} increase in $[SO_4^{2-}]_{(total)}$ within the range of 13–35 mmol kg^{-1} under approximate seawater conditions ([Ca $^{2+}$]_(total) = 10.28 mmol kg⁻¹, [B(OH)₄ + B(OH)₃] = 0.420 mmol kg⁻¹, [DIC] = 2.40 mmol kg⁻¹, [Cl⁻] = 550 mmol kg⁻¹, [Mg²⁺]_(total) = 52.8 mmol kg^{-1}) will result in a 2.5 to 7.5 % increase in $[CaSO_4^0]_{(aq)}$ with larger impact under low [SO₄²⁻]_(total) conditions. Following the same seawater concentrations, 1 mmol kg⁻¹ increase in $[Ca^{2+}]_{(total)}$ within the range of 5 to 23 mmol kg⁻¹ will induce an increase from 3.9 to 20 % in $[CaSO_4^0]_{(aq)}$ and indicates a larger change in $[CaSO_4^0]_{(aq)}$ when $[Ca^{2+}]_{(total)}$ is low (Fig. 6 a).

Studies investigating past seawater chemistry based on fluid inclusions (Horita et al., 2002 and references therein; Wortmann and Paytan, 2012) showed that seawater $[SO_4^2]_{(total)}$ was lower during the Mesozoic Era (252 – 66 Ma; https://stratigraphy.org), and during the warmer periods of the Cenozoic (66 Ma to present). At times of increased greenhouse concentrations, $[SO_4^2]_{(total)}$ may have been as low as 2.1 mmol kg⁻¹ (Wortmann and Paytan, 2012). Such an extreme decrease in $[SO_4^2]_{(total)}$ would cause a decrease of 860 µmol kg⁻¹ in $[CaSO_4^0]_{(aq)}$, which could contribute to somewhat lower S/Ca values in inorganic and biogenic carbonates. Concurrently, seawater $[Ca^{2+}]_{(total)}$ was shown to

be higher during the early Cenozoic and late Mesozoic and it may have reached concentrations of 50 mmol kg^{-1} between 60 Ma and 85 Ma (Wallmann, 2001). This elevation in seawater $[{\rm Ca}^{2+}]_{(total)}$ could result in a major increase in $[{\rm CaSO}_4^0]_{(aq)}$ as high as 2950 µmol kg^{-1} and, in combination with the reduction in $[{\rm SO}_4^{2-}]_{(total)}$, it could still cause a net increase in $S/{\rm Ca}_{(cc)}$ values. More moderate estimates suggest that seawater $[{\rm Ca}^{2+}]_{(total)}$ and $[{\rm SO}_4^{2-}]_{(total)}$ were 14 mmol kg^{-1} higher and 20 mmol kg^{-1} lower, respectively, at 150 Ma (Horita et al., 2002). These, in combination with the estimated decrease in $[{\rm Mg}^{2+}]_{(total)}$ (26 mmol kg^{-1} ; Horita et al., 2002) would reduce $[{\rm CaSO}_4^0]_{(aq)}$ by 205 µmol kg^{-1} with respect to the modern values (approximately 931 µmol kg^{-1}).

Our data from the pH - [Ca $^{2+}$] experimental series demonstrate a potential inverse relationship between S/Ca $_{\rm (cc)}$ and pH (Fig. 2 d), which is consistent with the results from culture experiments using benthic foraminifera (Van Dijk et al., 2017). However, pH does not contribute to a significant change in [CaSO $_{\rm 1(aq)}^0$. As shown in Fig. 6 b, within the range from 4 to 10, a pHNBS change by 1 unit result in less than 20 μ mol kg $^{-1}$ of change in [CaSO $_{\rm 1(aq)}^0$. The relation found between Ds and pH is therefore more likely related to a change in [Ca $^{2+}$](total), which has sizable impacts on [CaSO $_{\rm 1(aq)}^0$. More experiments, especially those with manipulations of only pH, are required to affirm if pH has an additional influence during the incorporation process.

Formation of sulfate complexes other than $CaSO_{4}^{0}$ will reduce the amount of free aqueous $[SO_{4}^{2-}]_{(aq)}$ available, which may either cause a decrease of the total amount of incorporated sulfate in calcite or may be compensated for via the incorporation of various sulfate complexes, such as $MgSO_{4}^{0}$. Ions of Mg^{2+} and SO_{4}^{2-} are likely incorporated in $CaCO_{3}$ via linked processes (Van Dijk et al., 2019a; Van Dijk et al., 2019b) which may even relate to their uptake as an ion pair (Sakuma et al., 2014). Based on the calculations in PHREEQC, we indeed see decreasing $[CaSO_{4}^{0}]_{(aq)}$ with increasing $[Mg^{2+}]_{(total)}$ but variation in $[Mg^{2+}]_{(total)}$ alone will contribute to only a minor change in $[CaSO_{4}^{0}]_{(aq)}$ (3–7 μ mol kg⁻¹ per 1 mmol kg⁻¹ change of $[Mg^{2+}]_{(total)}$) with respect to changes in either $[Ca^{2+}]_{(total)}$ or $[SO_{4}^{2-}]_{(total)}$ (Fig. 6 c).

4.7. The potential of foraminiferal S/Ca as a proxy for the carbon system

Comparison of inorganic calcite growth and foraminiferal culture experiments is complicated by different scales of precipitation rates typical for inorganically formed and biogenic calcium carbonates. Similar precipitation rate as within this study ($-5.40 \pm 0.1 \log_{10}$ mol m⁻² sec⁻¹) has been reported only from low-Mg/Ca foraminifera (Geerken et al., 2022), as the influence of precipitation rates on element incorporation is generally tested over a large and often higher range during inorganic growth experiments, compared to the rate at which foraminifera precipitate their calcite (Haynes et al., 2017 and references therein). The preferred polymorph that forms also depends on the conditions and is not necessarily the same within the calcifying space of a foraminifer and an inorganic precipitation experiment. Foraminifera approaching relatively high precipitation rate on their scales likely result from a high level of supersaturation. This in turn has been hypothesized to result in the formation of an amorphous precursor and hence affects the extent of element incorporation (Evans et al., 2020). Critically, $[SO_4^{2-}]_{(total)}$ and $[Mg^{2+}]_{(total)}$ of our experimental solutions were six times and twenty-five times lower than the respective concentration in natural seawater in order to avoid precipitation of CaCO₃ polymorphs other than calcite (most importantly aragonite). Thus, the potential contribution of free SO₄²⁻ ions versus ion-pairs, such as CaSO₄⁰ for D_s is difficult to scale for foraminiferal calcification. Moreover, certain organic molecules can interact with SO₄²⁻ near the site of calcification, adding further complications when comparing $D_{s}\mbox{ or }S/\mbox{Ca}_{(cc)}$ between inorganic and foraminiferal calcite. Combined foraminifera culture and inorganic experiments under various [Ca²⁺]_(total), [SO₄²⁻]_(total), [Mg²⁺]_(total) in future studies, however, have the potential to solidify the theoretical basis of the S/Ca_(cc) as a paleo-proxy and improve its applicability.

Even if foraminiferal S/Ca(cc) values alone cannot be used for reconstructing seawater carbon chemistry, as the results of this study imply, it may be used in combination with other elements that share (some of) the same controls on their incorporations or when growth rate and seawater chemistry is well-constrained. There is yet no proxy available to quantitatively determine precipitation/growth rate in fossil foraminifera, but alternative indicators are available to correct for precipitation rate effects. Sodium to calcium ratios in calcite have been shown to be strongly dependent on precipitation rate (Devriendt et al., 2021). If the influence of other parameters, such as salinity (Mezger et al., 2016; Wit et al., 2013) are minor on the Na/Ca(cc) values with respect to rate effects, this element could potentially be used to correct for the precipitation rate and isolate the influence of the carbon chemistry on the S/Ca_(cc) values. Alternatively, Sr/Ca_(cc) has been also shown to reflect growth rate (Cléroux et al., 2008; Keul et al., 2017; Kısakürek et al., 2008) and provide further constraints on the precipitation rate. In addition, the foraminiferal S/Ca_(cc) values may still have an application potential in environments where variation in precipitation/growth rate is minor, for instance in deep sea environments (e.g., Corliss and Silva, 1993; Gooday, 1994).

Fluctuations of $[Ca^{2+}]_{(total)}$ and $[SO_4^2-]_{(total)}$ over geological history need to be taken into account when $S/Ca_{(cc)}$ or D_s for (biogenic) calcite is used in pCO_2 reconstructions. While SO_4^2 has a residence time of about 15 million years in the ocean, Ca^{2+} has one of only 1.1 million years, thus limiting downcore application to less than 1 million years. Constraints on past $[Ca^{2+}]_{(total)}$ are hence important and may be provided based on fluid inclusions (Brennan et al., 2013; Horita et al., 2002) and Ca isotopes in foraminifera (Griffith et al., 2008; Heuser et al., 2005), but also based on element incorporations in foraminifera, such as Na/ $Ca_{(cc)}$ (Hauzer et al., 2018; Zhou et al., 2021) and K/ $Ca_{(cc)}$ (Nambiar et al., 2023).

Common planktonic foraminifera, such as Globigerinoides ruber, Globigerina bulloides, Trilobatus sacculifer, and Neogloboquadrina incompta, incorporate sulfate at a S/Ca(cc) ratio between 0.30 and 2.0 mmol mol⁻¹ (Karancz et al., 2024a), while benthic foraminifera show larger variability in S/Ca_(cc) values (Van Dijk et al., 2017). Miliolid foraminifera, such as Sorites marginalis, may have sulfate concentrations as high as 10 mmol mol⁻¹, whereas rotaliid foraminifera, e.g. Amphistegina gibbosa incorporate sulfate at ratios comparable to planktonic foraminifera (Van Dijk et al., 2017). The experiments performed using carbon chemistry conditions closest to natural seawater conditions ([DIC] = 2400 $\mu mol~kg^{-1}$, $pH_{NBS}=8.2$) resulted in three times higher sulfate incorporation compared to the high-S/Ca S. marginalis and twenty times higher than in planktonic and benthic rotaliid species. Miliolid foraminifera, however, likely build their shell using an internal reservoir which is not heavily modulated by active ion pumping, thus incorporating Mg, Sr, Na, Ba and SO_4^{2-} in ratios to Ca closer to the values observed for inorganic precipitation from seawater (de Nooijer et al., 2009; Van Dijk et al., 2017).

The lower S/Ca_(cc) ratios in foraminifera with respect to the levels observed for inorganic D_s emphasizes the microenvironmental controls related to the foraminifer' physiology. Calcification inherently requires a supersaturation with respect to CaCO_3 at the site of calcification, which potentially could involve an active removal or immobilization of ions inhibiting calcite growth, such as SO_4^{2-} and Mg^{2+} (Kontrec et al., 2004; Pokroy et al., 2006; Zeebe and Sanyal, 2002). As a consequence, less of these ions are available for incorporation and S/Ca and Mg/Ca of the newly formed calcite decrease.

During shell formation, Ca^{2+} is suggested to be pumped over the cell membrane into the site of calcification (de Nooijer et al., 2014; Evans et al., 2018; Higgins, 1992; Nehrke et al., 2013; Toyofuku et al., 2017). The site of calcification is isolated via a protective envelope from the surrounding seawater and the pH of the fluid in this site of calcification is modified by proton removal to increase $[\text{CO}_3^2]$ and saturation state, promoting calcite nucleation and growth. Consequently, and at constant seawater [DIC], the reduction in pH outside the foraminifer due to the

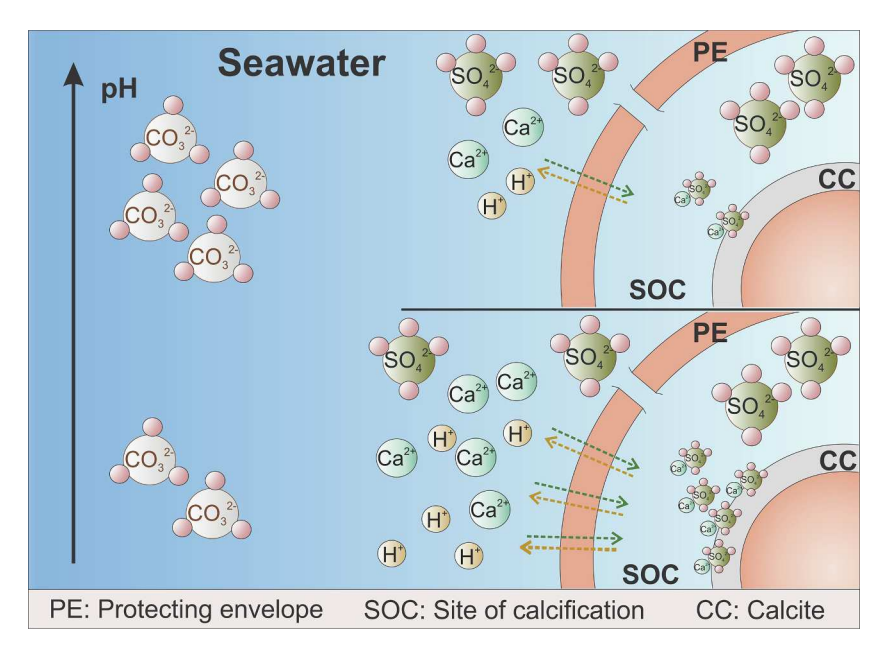


Fig. 7. Summary of sulfate incorporation in the form of $CaSO_4^0$ complex within the concept of hyaline foraminifera calcification (de Nooijer et al., 2014). Sulfate is likely taken up into the SOC via trans-membrane transport, but we here also depict the possibility of direct seawater transport and sulfate supply to the site of calcification. The $CaSO_4^0$ complex can be formed in the SOC fluid or be delivered to the SOC via direct seawater transport.

proton pumping will decrease the carbonate ion concentration. The large pH gradient (low outside, high inside the site of calcification) and the resulting large CO₂ gradient (high outside, low inside) is thought to promote the diffusion of carbon into the calcifying fluid and is accompanied by an inward Ca²⁺ flux that is coupled to the outward H⁺ pumping (likely in a ratio of 1:2; Toyofuku et al., 2017). It is still unresolved whether some seawater, containing amongst others also SO₄², is transported to the site of calcification through vacuoles (Bentov and Erez, 2006; Erez, 2003), or already present at the site of calcification at the onset of shell formation (de Nooijer et al., 2014; Geerken et al., 2022). Irrespective, it is clear from a mass balance consideration that active acquisition of Ca²⁺ at the site of calcification is needed to sustain the formation of calcium carbonate. Consequently, the elevated [Ca²⁺] at the site of calcification will increase CaSO₄ complexation and thus subsequently sulfate incorporation in the shell's calcite (Fig. 7). Such process forms a mechanistic link between $S/Ca_{(cc)}$ and $[CO_3^{2-}]_{(total)}$, as at lower pH (and thus carbonate ion concentration), more pumping is required to reach the Ω values needed to precipitate calcium carbonate at the rates observed. Although the total concentration of S will remain the same, it is unlikely that sulfate uptake through the cell membrane occurs in the form of the CaSO₄ complex due to its large size and neutral charge, but the formation of these complexes increases with [Ca²⁺]_{total} in the calcifying space. This could explain the negative correlation between S/Ca and [CO₃²⁻] (and pH) observed in benthic foraminiferal culture experiments (Van Dijk et al., 2017). Calibrating this potential proxy using field samples, however, showed that other parameters likely largely overprint such a primary signal. Other potential parameters affecting sulfate incorporation in foraminifera shells therefore remain subject to further research. For instance, an indirect effect of temperature, via competition between CaSO₄⁰ and MgSO₄⁰ may be responsible, but exploring the ratio of S to Mg may potentially provide an alternative approach to develop an independent seawater carbon system proxy.

5. Conclusions

Inorganic calcite growth experiments were performed in a simplified solution with respect to natural seawater conditions to understand the basic relations of sulfate incorporation with the carbonate system and growth-rate effects. The partition coefficient of sulfur shows a

dependence on calcite saturation state and / or precipitation rate, and on the carbon system via the changing solution pH. However, it remains to be tested whether pH or the changing solution chemistry (e.g., $[SO_4^2^-]/[CO_3^2^-]$) drives sulfate partitioning. Counterintuitively, calcite $S/Ca_{(cc)}$ values do not correlate positively with free aqueous $[SO_4^2^-]$ as expected based on former observations, but they reveal a positive trend with the aqueous $CaSO_4^0$ complex. These results are hinting at incorporation pathways other than (only) substitution of $SO_4^{2^-}$ for $CO_3^{2^-}$ in the calcite lattice and suggest that complexes formed with Ca^{2^+} (and potentially with Mg^{2^+}) in the solution may drive sulfate (and potentially also Mg^{2^+}) uptake in calcite and likely other calcium carbonate minerals. Investigating complexation affinity of cations and anions may be a key to better understanding primary controls in element incorporation in calcium carbonates and may provide the missing link for resolving discrepancies in multi-proxy reconstructions.

Data availability

Data are available through NIOZ Data Archive System at https://doi.org/10.25850/nioz/7b.b.yg (Karancz et al., 2024b).

CRediT authorship contribution statement

Szabina Karancz: Writing – original draft, Investigation, Data curation, Conceptualization. Joji Uchikawa: Writing – review & editing, Resources, Investigation, Data curation. Lennart J. de Nooijer: Writing – review & editing, Data curation, Conceptualization. Mariëtte Wolthers: Writing – review & editing, Data curation. Kyle A. Conner: Writing – review & editing, Investigation. Corinne G. Hite: Writing – review & editing, Supervision, Resources. Shiv K. Sharma: Writing – review & editing, Resources. Gert-Jan Reichart: Writing – review & editing, Supervision, Resources, Conceptualization.

Declaration of competing interest

The authors declare that they have no known competing financial interests or personal relationships that could have appeared to influence the work reported in this paper.

Acknowledgments

This work was carried out under the program of the Netherlands Earth System Science Centre (NESSC), financially supported by the Ministry of Education, Culture and Science (OCW) and the European Union's Horizon 2020 research and innovation program under the Marie Skłodowska-Curie, grant agreement No. [847504]. This project has received funding from the European Research Council (ERC) under the European Union's Horizon 2020 research and innovation program (grant agreement No. [819588]) to MW and U.S. NSF awards (OCE-2024631, OCE-2048436, EAR-2001927 and EAR-2323221) to JU, SS, and/or REZ provided support for the UH-based researchers. We wish to acknowledge Patrick Laan, Piet van Gaever and Wim Boer for the technical support during the sample analysis.

Appendix A. Supplementary material

The supplementary file associated with this manuscript contains: Figures and description of $El/Ca_{(cc)}$ data that were analyzed in addition to $S/Ca_{(cc)}$; Raman spectrum of one sample showing the characteristic peaks of calcite; Calculated error in $El/Ca_{(cc)}$ values based on $\delta^{13}C$ error; $S/Ca_{(cc)}$ values plotted against log activity ratio of SO_4^{2-} and CO_3^{2-} ; $S/Ca_{(cc)}$ values plotted against concentrations of various sulfate species $([SO_4^{2-}]_{(aq)}, [CaSO_4^0]_{(aq)}, [MgSO_4^0]_{(aq)}, [NaSO_4^-]_{(aq)})$ in the solution. Supplementary material to this article can be found online at htt ps://doi.org/10.1016/j.gca.2024.07.034.

References

- Allen, K.A., Hönisch, B., 2012. The planktic foraminiferal B/Ca proxy for seawater carbonate chemistry: a critical evaluation. Earth. Planet. Sci. Lett. 345–348, 203, 211
- Allen, K.A., Hönisch, B., Eggins, S.M., Rosenthal, Y., 2012. Environmental controls on B/Ca in calcite tests of the tropical planktic foraminifer species *Globigerinoides ruber* and *Globigerinoides sacculifer*. Earth. Planet. Sci. Lett. 351, 270–280.
- Amankonah, J.O., Somasundaran, P., 1985. Effects of dissolved mineral species on the electrokinetic behavior of calcite and apatite. Colloids Surf. 15, 335–353.
- Anand, P., Elderfield, H., Conte, M.H., 2003. Calibration of Mg/Ca thermometry in planktonic foraminifera from a sediment trap time series. Paleoceanography 18, 1050.
- Arroyo-de Dompablo, M.E., Fernández-González, M.A., Fernández-Díaz, L., 2015.

 Computational, investigation of the influence of tetrahedral oxoanions (sulphate, selenate and chromate) on the stability of calcium carbonate polymorphs. RSC Advances 5, 59845–59852.
- Babila, T.L., Rosenthal, Y., Conte, M.H., 2014. Evaluation of the biogeochemical controls on B/Ca of *Globigerinoides ruber* white from the Oceanic Flux Program, Bermuda. Earth. Planet. Sci. Lett. 404, 67–76.
- Barkan, Y., Paris, G., Webb, S.M., Adkins, J.F., Halevy, I., 2020. Sulfur isotope fractionation between aqueous and carbonate-associated sulfate in abiotic calcite and aragonite. Geochim. Cosmochim. Acta 280, 317–339.
- Bemis, B.E., Spero, H.J., Bijma, J., Lea, D.W., 1998. Reevaluation of the oxygen isotopic composition of planktonic foraminifera: experimental results and revised paleotemperature equations. Paleoceanography 13, 150–160.
- Bentov, S., Erez, J., 2006. Impact of biomineralization processes on the Mg content of foraminiferal shells: a biological perspective. Geochem. Geophys. Geosyst. 7.
- Blue, C.R., Dove, P.M., 2015. Chemical controls on the magnesium content of amorphous calcium carbonate. Geochim. Cosmochim. Acta 148, 23–33.
- Blue, C.R., Giuffre, A., Mergelsberg, S., Han, N., De Yoreo, J.J., Dove, P.M., 2017. Chemical and physical controls on the transformation of amorphous calcium carbonate into crystalline CaCO₃ polymorphs. Geochim. Cosmochim. Acta 196, 179–196.
- Boer, W., Nordstad, S., Weber, M., Mertz-Kraus, R., Hönisch, B., Bijma, J., Raitzsch, M., Wilhelms-Dick, D., Foster, G.L., Goring-Harford, H., 2022. New calcium carbonate nano-particulate pressed powder pellet (NFHS-2-NP) for LA-ICP-OES, LA-(MC)-ICP-MS and μXRF. Geostand. Geoanalytical Res. 46, 411–432.
- Bots, P., Benning, L.G., Rickaby, R.E.M., Shaw, S., 2011. The role of SO_4 in the switch from calcite to aragonite seas. Geology 39, 331–334.
- Brennan, S.T., Lowenstein, T.K., Cendon, D.I., 2013. The major-ion composition of Cenozoic seawater: The past 36 million years from fluid inclusions in marine halite. Am. J. Sci. 313, 713–775.
- Busenberg, E., Plummer, L.N., 1985. Kinetic and thermodynamic factors controlling the distribution of SO₄²⁻ and Na⁺ in calcites and selected aragonites. Geochim. Cosmochim. Acta 49, 713–725.
- Byrne, R.H., 2003. Inorganic speciation of dissolved elements in seawater: the influence of pH on concentration ratios. Geochem. Trans. 3, 11–16.

- Cicerone, D.S., Regazzoni, A.E., Blesa, M.A., 1992. Electrokinetic properties of the calcite/water interface in the presence of magnesium and organic matter. J. Colloid Interface Sci. 154, 423–433.
- Cléroux, C., Cortijo, E., Anand, P., Labeyrie, L., Bassinot, F., Caillon, N., Duplessy, J.C., 2008. Mg/Ca and Sr/Ca ratios in planktonic foraminifera: Proxies for upper water column temperature reconstruction. Paleoceanography 23.
- Conner, K., Sharma, S., Uchiyama, R., Tanaka, K., Murakami-Sugihara, N., Shirai, K., Kahng, S., 2023. Raman analysis of octocoral carbonate ion structural disorder along a natural depth gradient, Kona coast. Hawai'i 108, 999–1013.
- Corliss, B., Silva, K.A., 1993. Rapid growth of deep-sea benthic foraminifera. Geology 21, 991–994.
- Davis, K.J., Dove, P.M., Wasylenki, L.E., De Yoreo, J.J., 2004. Morphological consequences of differential Mg^{2+} incorporation at structurally distinct steps on calcite. Am. Mineral. 89, 714–720.
- de Nooijer, L.J., Toyofuku, T., Kitazato, H., 2009. Foraminifera promote calcification by elevating their intracellular pH. Proc. Natl Acad. Sci. USA 106, 15374–15378.
- de Nooijer, L.J., Spero, H., Erez, J., Bijma, J., Reichart, G.-J., 2014. Biomineralization in Perforate Foraminifera. Earth-Sci. Rev. 135, 48–58.
- de Villiers, S., Greaves, M., Elderfield, H., 2002. An intensity ratio calibration method for the accurate determination of Mg/Ca and Sr/Ca of marine carbonates by ICP-AES. Geochem. Geophys. Geosyst. 3.
- DeCarlo, T.M., 2018. Characterizing coral skeleton mineralogy with Raman spectroscopy. Nat. Commun. 9, 5325.
- Dekens, P.S., Ravelo, A.G., McCarthy, M.D., Edwards, C.A., 2008. A 5 million year comparison of Mg/Ca and alkenone paleothermometers. Geochem. Geophys. Geosyst. 9.
- DePaolo, D.J., 2011. Surface kinetic model for isotopic and trace element fractionation during precipitation of calcite from aqueous solutions. Geochim. Cosmochim. Acta 75, 1039–1056.
- Devriendt, L., Mezger, E., Olsen, E., Watkins, J., Kaczmarek, K., Nehrke, G., De Nooijer, L., Reichart, G.-J., 2021. Sodium incorporation into inorganic $CaCO_3$ and implications for biogenic carbonates. Geochim. Cosmochim. Acta 314, 294–312.
- Epstein, S., Buchsbaum, R., Lowenstam, H.A., Urey, H.C., 1953. Revised carbonate-water isotopic temperature scale. GSA Bulletin 64, 1315–1326.
- Erez, J., 2003. The source of ions for biomineralization in foraminifera and their implications for paleoceanographic proxies. Rev. Mineral. Geochem. 54, 115–149.
- Evans, R.C., 1966. An introduction to crystal chemistry. Cambridge University Press, Cambridge.
- Evans, D., Wade, B.S., Henehan, M., Erez, J., Müller, W., 2016. Revisiting carbonate chemistry controls on planktic foraminifera Mg/Ca: implications for sea surface temperature and hydrology shifts over the Paleocene-Eocene Thermal Maximum and Eocene-Oligocene transition. Clim. past 12, 819–835.
- Evans, D., Müller, W., Erez, J., 2018. Assessing foraminifera biomineralisation models through trace element data of cultures under variable seawater chemistry. Geochim. Cosmochim. Acta 236, 198–217.
- Evans, D., Gray, W.R., Rae, J.W.B., Greenop, R., Webb, P.B., Penkman, K., Kröger, R., Allison, N., 2020. Trace and major element incorporation into amorphous calcium carbonate (ACC) precipitated from seawater. Geochim. Cosmochim. Acta 290, 293–311.
- Fernández-Díaz, L., Fernández-González, Á., Prieto, M., 2010. The role of sulfate groups in controlling $CaCO_3$ polymorphism. Geochim. Cosmochim. Acta 74, 6064–6076.
- Foster, G.L., 2008. Seawater pH, pCO_2 and $[CO_3^2]$ variations in the Caribbean Sea over the last 130 kyr: a boron isotope and B/Ca study of planktic foraminifera. Earth. Planet. Sci. Lett. 271, 254–266.
- Foxall, T., Peterson, G.C., Rendall, H.M., Smith, A.L., 1979. Charge determination at calcium salt/aqueous solution interface. J. Chem. Soc., Faraday Trans. 1: Phys. Chem. Condensed Phases 75, 1034–1039.
- Frisia, S., Borsato, A., Fairchild, I.J., Susini, J., 2005. Variations in atmospheric sulphate recorded in stalagmites by synchrotron micro-XRF and XANES analyses. Earth. Planet. Sci. Lett. 235, 729–740.
- Garrels, R.M., Thompson, M.E., 1962. A chemical model for sea water at 25°C and one atmosphere total pressure. Am. J. Sci. 260, 57–66.
- Geerken, E., de Nooijer, L., Toyofuku, T., Roepert, A., Middelburg, J.J., Kienhuis, M.V., Nagai, Y., Polerecky, L., Reichart, G.-J., 2022. High precipitation rates characterize biomineralization in the benthic foraminifer *Ammonia beccarii*. Geochim. Cosmochim. Acta 318, 70–82.
- Giuffre, A.J., Gagnon, A.C., De Yoreo, J.J., Dove, P.M., 2015. Isotopic tracer evidence for the amorphous calcium carbonate to calcite transformation by dissolution–reprecipitation. Geochim. Cosmochim. Acta 165, 407–417.
- Goetschl, K.E., Purgstaller, B., Dietzel, M., Mavromatis, V., 2019. Effect of sulfate on magnesium incorporation in low-magnesium calcite. Geochim. Cosmochim. Acta 265, 505–519.
- Goetschl, K.E., Dietzel, M., Purgstaller, B., Grengg, C., Μαυρομάτης, B., 2021. Control of MgSO_{4(aq)} on the transformation of amorphous calcium carbonate to high-Mg calcite and long-term reactivity of the crystalline solid. Geochim. Cosmochim. Acta 312, 357–374.
- Gooday, A.J., 1994. The biology of deep-sea for aminifera: a review of some advances and their applications in paleocean ography. Palaios 9, 14–31.
- Grasby, S.E., 2003. Naturally precipitating vaterite (μ-CaCO₃) spheres: unusual carbonates formed in an extreme environment. Geochim. Cosmochim. Acta 67, 1659–1666.
- Gray, W.R., Evans, D., 2019. Nonthermal influences on Mg/Ca in planktonic foraminifera: A review of culture studies and application to the last glacial maximum. Paleoceanogr. Paleoclimatol. 34, 306–315.
- Gray, W.R., Weldeab, S., Lea, D.W., Rosenthal, Y., Gruber, N., Donner, B., Fischer, G., 2018. The effects of temperature, salinity, and the carbonate system on Mg/Ca in

- *Globigerinoides ruber* (white): a global sediment trap calibration. Earth. Planet. Sci. Lett. 482, 607–620.
- Griffith, E.M., Paytan, A., Kozdon, R., Eisenhauer, A., Ravelo, A.C., 2008. Influences on the fractionation of calcium isotopes in planktonic foraminifera. Earth. Planet. Sci. Lett. 268, 124–136.
- Grossman, E.L., Mii, H.-S., Zhang, C., Yancey, T.E., 1996. Chemical variation in Pennsylvanian brachiopod shells; diagenetic, taxonomic, microstructural, and seasonal effects. J. Sediment. Res. 66, 1011–1022.
- Guo, J., Li, T., Xiong, Z., Qiu, X., Chang, F., 2019. Revisiting the dependence of thermocline-dwelling foraminiferal B/Ca on temperature and [CO₃²⁻], and its application in reconstruction of the subsurface carbonate system in the tropical western Pacific since 24 ka. Acta Oceanol. Sin. 38, 71–86.
- Harris, C.R., Millman, K.J., van der Walt, S.J., Gommers, R., Virtanen, P., Cournapeau, D., Wieser, E., Taylor, J., Berg, S., Smith, N.J., Kern, R., Picus, M., Hoyer, S., van Kerkwijk, M.H., Brett, M., Haldane, A., del Río, J.F., Wiebe, M., Peterson, P., Gérard-Marchant, P., Sheppard, K., Reddy, T., Weckesser, W., Abbasi, H., Gohlke, C., Oliphant, T.E., 2020. Array programming with NumPy. Nature 585, 357–362.
- Hauzer, H., Evans, D., Müller, W., Rosenthal, Y., Erez, J., 2018. Calibration of Na partitioning in the calcitic foraminifer *Operculina ammonoides* under variable Ca concentration: Toward reconstructing past seawater composition. Earth. Planet. Sci. Lett. 497, 80–91.
- Haynes, L.L., Hönisch, B., Dyez, K.A., Holland, K., Rosenthal, Y., Fish, C.R., Subhas, A.V., Rae, J.W., 2017. Calibration of the B/Ca proxy in the planktic foraminifer *Orbulina universa* to Paleocene seawater conditions. Paleoceanography 32, 580–599.
- Hemming, N., Hanson, G., 1992. Boron isotopic composition and concentration in modern marine carbonates. Geochim. Cosmochim. Acta 56, 537–543.
- Henehan, M.J., Foster, G.L., Rae, J.W., Prentice, K.C., Erez, J., Bostock, H.C., Marshall, B. J., Wilson, P.A., 2015. Evaluating the utility of B/C a ratios in planktic foraminifera as a proxy for the carbonate system: a case study of *Globigerinoides ruber*. Geochem. Geophys. Geosyst. 16, 1052–1069.
- Heuser, A., Eisenhauer, A., Böhm, F., Wallmann, K., Gussone, N., Pearson, P.N.,
 Nägler, T.F., Dullo, W.-C., 2005. Calcium isotope (8⁴⁴/⁴⁰Ca) variations of Neogene planktonic foraminifera. Paleoceanography 20.
- Higgins, C.F., 1992. ABC transporters: from microorganisms to man. Annu. Rev. Cell Biol. 8. 67–113.
- Horita, J., Zimmermann, H., Holland, H.D., 2002. Chemical evolution of seawater during the Phanerozoic: Implications from the record of marine evaporites. Geochim. Cosmochim. Acta 66, 3733–3756.
- Karancz, S., de Nooijer, L.J., Brummer, G.J.A., Lattaud, J., Haghipour, N., Rosenthal, Y., Reichart, G.J., 2024a. Impact of seawater inorganic carbon chemistry on element incorporation in foraminiferal shell carbonate. Geochem. Geophys. Geosyst. 25, e2023GC011302.
- Karancz, S., Uchikawa, J., de Nooijer, L.J., Wolthers, M.t., Conner, K.A., Hite, C.G., Zeebe, R.E., Sharma, S., Reichart, G.-J., 2024b. Dataset belonging to "Constraining sulfur incorporation in calcite using controlled growth experiments", V2 ed. NIOZ.
- Keul, N., Langer, G., de Nooijer, L.J., Nehrke, G., Reichart, G.J., Bijma, J., 2013. Incorporation of uranium in benthic foraminiferal calcite reflects seawater carbonate ion concentration. Geochem. Geophys. Geosyst. 14, 102–111.
- Keul, N., Langer, G., Thoms, S., de Nooijer, L.J., Reichart, G.-J., Bijma, J., 2017. Exploring foraminiferal Sr/Ca as a new carbonate system proxy. Geochim. Cosmochim. Acta 202, 374–386.
- Kısakürek, B., Eisenhauer, A., Böhm, F., Garbe-Schönberg, D., Erez, J., 2008. Controls on shell Mg/Ca and Sr/Ca in cultured planktonic foraminiferan, *Globigerinoides ruber* (white). Earth. Planet. Sci. Lett. 273, 260–269.
- Konrad, F., Gallien, F., Gerard, D.E., Dietzel, M., 2016. Transformation of Amorphous Calcium Carbonate in Air. Cryst. Growth Des. 16, 6310–6317.
- Konrad, F., Purgstaller, B., Gallien, F., Mavromatis, V., Gane, P., Dietzel, M., 2018. Influence of aqueous Mg concentration on the transformation of amorphous calcium carbonate. J. Cryst. Growth 498, 381–390.
- Kontrec, J., Kralj, D., Brečević, L., Falini, G., Fermani, S., Noethig-Laslo, V., Mirosavljević, K., 2004. Incorporation of inorganic anions in calcite. Eur. J. Inorg. Chem. 2004, 4579–4585.
- Kralj, D., Kontrec, J., Brečević, L., Falini, G., Nöthig-Laslo, V., 2004. Effect of inorganic anions on the morphology and structure of magnesium calcite. Chem. – A Eur. J. 10, 1647–1656.
- Laepple, T., Huybers, P., 2013. Reconciling discrepancies between Uk37 and Mg/Ca reconstructions of Holocene marine temperature variability. Earth. Planet. Sci. Lett. 375, 418–429.
- Larsen, K., Bechgaard, K., Stipp, S.L.S., 2010. Modelling spiral growth at dislocations and determination of critical step lengths from pyramid geometries on calcite 101⁻⁴ surfaces. Geochim. Cosmochim. Acta 74, 558–567.
- Lea, D.W., Mashiotta, T.A., Spero, H.J., 1999. Controls on magnesium and strontium uptake in planktonic foraminifera determined by live culturing. Geochim. Cosmochim. Acta 63, 2369–2379.
- Lorens, R.B., Bender, M.L., 1980. The impact of solution chemistry on Mytilus edulis calcite and aragonite. Geochim. Cosmochim. Acta 44, 1265–1278.
- Martinez-Boti, M.A., Marino, G., Foster, G.L., Ziveri, P., Henehan, M.J., Rae, J.W., Mortyn, P.G., Vance, D., 2015. Boron isotope evidence for oceanic carbon dioxide leakage during the last deglaciation. Nature 518, 219–222.
- Maslen, E., Streltsov, V., Streltsova, N., Ishizawa, N., 1995. Electron density and optical anisotropy in rhombohedral carbonates. III. Synchrotron X-ray studies of CaCO₃, MgCO₃ and MnCO₃. Acta Crystallogr. Sect. b: Struct. Sci. 51, 929–939.
- Mejri, W., Korchef, A., Tlili, M., Ben, A.M., 2014. Effects of temperature on precipitation kinetics and microstructure of calcium carbonate in the presence of magnesium and sulphate ions. Desalin. Water Treat. 52, 4863–4870.

- Mewes, A., Langer, G., Reichart, G.-J., de Nooijer, L.J., Nehrke, G., Bijma, J., 2015. The impact of Mg contents on Sr partitioning in benthic foraminifers. Chem. Geol. 412, 92–98
- Meyer, H., 1984. The influence of impurities on the growth rate of calcite. J. Cryst. Growth 66, 639–646.
- Mezger, E., De Nooijer, L., Boer, W., Brummer, G., Reichart, G., 2016. Salinity controls on Na incorporation in Red Sea planktonic foraminifera. Paleoceanography 31, 1562–1582.
- Midgley, S.D., Taylor, J.O., Fleitmann, D., Grau-Crespo, R., 2020. Molybdenum and sulfur incorporation as oxyanion substitutional impurities in calcium carbonate minerals: a computational investigation. Chem. Geol. 553, 119796.
- Mills, J.V., Barnhart, H.A., DePaolo, D.J., Lammers, L.N., 2022. New insights into Mn²⁺ and Mg²⁺ inhibition of calcite growth. Geochim. Cosmochim. Acta 334, 338–367.
- Mucci, A., Canuel, R., Zhong, S., 1989. The solubility of calcite and aragonite in sulfate-free seawater and the seeded growth kinetics and composition of the precipitates at 25 C. Chem. Geol. 74, 309–320.
- Nambiar, R., Hauzer, H., Gray, W.R., Henehan, M.J., Cotton, L., Erez, J., Rosenthal, Y., Renema, W., Müller, W., Evans, D., 2023. Controls on potassium incorporation in foraminifera and other marine calcifying organisms. Geochim. Cosmochim. Acta 351, 125–138.
- Nehrke, G., Keul, N., Langer, G., de Nooijer, L.J., Bijma, J., Meibom, A., 2013. A new model for biomineralization and trace-element signatures of Foraminifera tests. Biogeosciences 10, 6759–6767.
- Nielsen, M.H., Aloni, S., De Yoreo, J.J., 2014. In situ TEM imaging of CaCO₃ nucleation reveals coexistence of direct and indirect pathways. Science 345, 1158–1162.
- Nielsen, L.C., De Yoreo, J.J., DePaolo, D.J., 2013. General model for calcite growth kinetics in the presence of impurity ions. Geochim. Cosmochim. Acta 115, 100–114.
- Nielsen, M., Sand, K.K., Rodriguez-Blanco, J.D., Bovet, N., Generosi, J., Dalby, K., Stipp, S., 2016. Inhibition of calcite growth: combined effects of ${\rm Mg}^{2+}$ and ${\rm SO_4^{2-}}$. Cryst. Growth Des. 16, 6199–6207.
- Okai, T., Suzuki, A., Terashima, S., Inoue, M., Nohara, M., Kawahata, H., Imai, N., 2004. Collaborative analysis of GSJ/AIST geochemical reference materials JCp-1 (Coral) and JCt-1 (Giant Clam). Geochem 38, 281–286.
- Okumura, T., Kim, H.-J., Kim, J.-W., Kogure, T., 2018. Sulfate-containing calcite: crystallographic characterization of natural and synthetic materials. Eur. J. Mineral. 30, 929–937
- Okumura, M., Kitano, Y., 1986. Coprecipitation of alkali metal ions with calcium carbonate. Geochim. Cosmochim. Acta 50, 49–58.
- Ossorio, M., Van Driessche, A.E.S., Pérez, P., García-Ruiz, J.M., 2014. The gypsum–anhydrite paradox revisited. Chem. Geol. 386, 16–21.
- Palmer, M.R., Brummer, G.J., Cooper, M.J., Elderfield, H., Greaves, M.J., Reichart, G.J., Schouten, S., Yu, J.M., 2010. Multi-proxy reconstruction of surface water pCO₂ in the northern Arabian Sea since 29 ka. Earth. Planet. Sci. Lett. 295, 49–57.
- Paquette, J., Reeder, R.J., 1990. New type of compositional zoning in calcite: Insights into crystal-growth mechanisms. Geology 18, 1244.
- Parkhurst, D.L., Appelo, C.A.J., 1999. User's guide to PHREEQC (Version 2): a computer program for speciation, batch-reaction, one-dimensional transport, and inverse geochemical calculations. Water-Resources Investigations Report 99, 312.
- Piana, S., Jones, F., Gale, J.D., 2006. Assisted desolvation as a key kinetic step for crystal growth. J. Am. Chem. Soc. 128, 13568–13574.
- Pingitore, N.E., Meitzner, G., Love, K.M., 1995. Identification of sulfate in natural carbonates by X-ray absorption spectroscopy. Geochim. Cosmochim. Acta 59, 2477–2483.
- Pokroy, B., Fitch, A.N., Marin, F., Kapon, M., Adir, N., Zolotoyabko, E., 2006. Anisotropic lattice distortions in biogenic calcite induced by intra-crystalline organic molecules. J. Struct. Biol. 155. 96–103.
- Prieto-Taboada, N., Gómez-Laserna, O., Martínez-Arkarazo, I., Olazabal, M.Á., Madariaga, J.M., 2014. Raman spectra of the different phases in the $CaSO_4-H_2O$ system. Anal. Chem. 86, 10131–10137.
- Radha, A.V., Forbes, T.Z., Killian, C.E., Gilbert, P.U.P.A., Navrotsky, A., 2010. Transformation and crystallization energetics of synthetic and biogenic amorphous calcium carbonate. Proc. Natl. Acad. Sci. 107, 16438–16443.
- Raitzsch, M., Kuhnert, H., Hathorne, E.C., Groeneveld, J., Bickert, T., 2011. U/Ca in benthic foraminifers: a proxy for the deep-sea carbonate saturation. Geochem. Geophys. Geosyst. 12.
- Romanek, C.S., Grossman, E.L., Morse, J.W., 1992. Carbon isotopic fractionation in synthetic aragonite and calcite: Effects of temperature and precipitation rate. Geochim. Cosmochim. Acta 56, 419–430.
- Rosenthal, Y., Lohmann, G., Lohmann, K., Sherrell, R., 2000. Incorporation and preservation of Mg in *Globigerinoides sacculifer*: Implications for reconstructing the temperature and $^{18}\text{O}/^{16}\text{O}$ of seawater. Paleoceanography 15, 135–145.
- Russell, A.D., Hönisch, B., Spero, H.J., Lea, D.W., 2004. Effects of seawater carbonate ion concentration and temperature on shell U, Mg, and Sr in cultured planktonic foraminifera. Geochim. Cosmochim. Acta 68, 4347–4361.
- Sakuma, H., Andersson, M.P., Bechgaard, K., Stipp, S.L.S., 2014. Surface tension alteration on calcite, induced by ion substitution. J. Phys. Chem. C 118, 3078–3087.
- Sanyal, A., Nugent, M., Reeder, R., Bijma, J., 2000. Seawater pH control on the boron isotopic composition of calcite: evidence from inorganic calcite precipitation experiments. Geochim. Cosmochim. Acta 64, 1551–1555.
- Schmid, T., Jungnickel, R., Dariz, P., 2020. Insights into the CaSO₄–H₂O system: A Raman-spectroscopic study. Minerals 10, 115–148.
- Siffert, D., Fimbel, P., 1984. Parameters affecting the sign and magnitude of the eletrokinetic potential of calcite. Colloids Surf. 11, 377–389.
- Somasundaran, P., Agar, G.E., 1967. The zero point of charge of calcite. J. Colloid Interface Sci. 24, 433–440.

- Takano, B., 1985. Geochemical implications of sulfate in sedimentary carbonates. Chem. Geol. 49, 393–403.
- Takano, B., Asano, Y., Watanuki, K., 1980. Characterization of sulfate ion in travertine. Contrib. Mineral. Petrol. 72, 197–203.
- Tang, Y., Zhang, F., Cao, Z., Jing, W., Chen, Y., 2012. Crystallization of $CaCO_3$ in the presence of sulfate and additives: Experimental and molecular dynamics simulation studies. J. Colloid Interface Sci. 377, 430–437.
- Teng, H.H., Dove, P.M., De Yoreo, J.J., 2000. Kinetics of calcite growth: surface processes and relationships to macroscopic rate laws. Geochim. Cosmochim. Acta 64, 2255–2266.
- Toyofuku, T., Matsuo, M.Y., de Nooijer, L.J., Nagai, Y., Kawada, S., Fujita, K., Reichart, G.-J., Nomaki, H., Tsuchiya, M., Sakaguchi, H., Kitazato, H., 2017. Proton pumping accompanies calcification in foraminifera. Nat. Commun. 8, 14145.
- Uchikawa, J., Penman, D.E., Zachos, J.C., Zeebe, R.E., 2015. Experimental evidence for kinetic effects on B/Ca in synthetic calcite: implications for potential B(OH)₄ and B (OH)₃ incorporation. Geochim. Cosmochim. Acta 150, 171–191.
- Uchikawa, J., Harper, D.T., Penman, D.E., Zachos, J.C., Zeebe, R.E., 2017. Influence of solution chemistry on the boron content in inorganic calcite grown in artificial seawater. Geochim. Cosmochim. Acta 218, 291–307.
- Uchikawa, J., Penman, D.E., Harper, D.T., Farmer, J.R., Zachos, J.C., Planavsky, N.J., Zeebe, R.E., 2023. Sulfate and phosphate oxyanions alter B/Ca and δ^{11} B in inorganic calcite at constant pH: Crystallographic controls outweigh normal kinetic effects. Geochim. Cosmochim. Acta 343, 353–370.
- Van Dijk, I., de Nooijer, L.J., Boer, W., Reichart, G.-J., 2017. Sulfur in foraminiferal calcite as a potential proxy for seawater carbonate ion concentration. Earth. Planet. Sci. Lett. 470, 64–72.
- Van Dijk, I., Barras, C., De Nooijer, L.J., Mouret, A., Geerken, E., Oron, S., Reichart, G.-J., 2019a. Coupled calcium and inorganic carbon uptake suggested by magnesium and sulfur incorporation in foraminiferal calcite. Biogeosciences 16, 2115–2130.
- Van Dijk, I., Mouret, A., Cotte, M., Le Houedec, S., Oron, S., Reichart, G.-J., Reyes-Herrera, J., Filipsson, H.L., Barras, C., 2019b. Chemical heterogeneity of Mg, Mn, Na, S, and Sr in benthic foraminiferal calcite. Front. Earth Sci. 7, 281.
- Walker, J.M., Marzec, B., Nudelman, F., 2017. Solid-state transformation of amorphous calcium carbonate to aragonite captured by cryoTEM. Angew. Chem. Int. Ed. 56, 11740–11743.
- Wallmann, K., 2001. Controls on the cretaceous and cenozoic evolution of seawater composition, atmospheric CO₂ and climate. Geochim. Cosmochim. Acta 65, 3005–3025.

- Wit, J.C., de Nooijer, L.J., Wolthers, M., Reichart, G.J., 2013. A novel salinity proxy based on Na incorporation into foraminiferal calcite. Biogeosciences 10, 6375–6387.
- Wolthers, M., Charlet, L., Van Cappellen, P., 2008. The surface chemistry of divalent metal carbonate minerals; a critical assessment of surface charge and potential data using the charge distribution multi-site ion complexation model. Am. J. Sci. 308, 905–941.
- Wolthers, M., Nehrke, G., Gustafsson, J.P., Van Cappellen, P., 2012. Calcite growth kinetics: Modeling the effect of solution stoichiometry. Geochim. Cosmochim. Acta 77, 121–134.
- Wortmann, U.G., Paytan, A., 2012. Rapid variability of seawater chemistry over the past 130 Million years. Science 337, 334–336.
- Wynn, P.M., Fairchild, I.J., Borsato, A., Spötl, C., Hartland, A., Baker, A., Frisia, S., Baldini, J.U., 2018. Sulphate partitioning into calcite: Experimental verification of pH control and application to seasonality in speleothems. Geochim. Cosmochim. Acta 226, 69–83.
- Yang, Y., Sahai, N., Romanek, C.S., Chakraborty, S., 2012. A computational study of Mg² dehydration in aqueous solution in the presence of HS⁻ and other monovalent anions Insights to dolomite formation. Geochim. Cosmochim. Acta 88, 77–87.
- Yu, J., Elderfield, H., 2007. Benthic foraminiferal B/Ca ratios reflect deep water carbonate saturation state. Earth. Planet. Sci. Lett. 258, 73–86.
- Yu, J., Elderfield, H., Hönisch, B., 2007. B/Ca in planktonic foraminifera as a proxy for surface seawater pH. Paleoceanography 22.
- Zeebe, R.E., Sanyal, A., 2002. Comparison of two potential strategies of planktonic foraminifera for house building: Mg²⁺ or H⁺ removal? Geochim. Cosmochim. Acta 66, 1159–1169.
- Zeebe, R.E., Tyrrell, T., 2019. History of carbonate ion concentration over the last 100 million years II: Revised calculations and new data. Geochim. Cosmochim. Acta 257, 373–392
- Zeebe, R.E., Wolf-Gladrow, D., 2001. CO₂ in seawater: Equilibrium, kinetics, isotopes. Elsevier, Amsterdam.
- Zhou, X., Rosenthal, Y., Haynes, L., Si, W., Evans, D., Huang, K.-F., Hönisch, B., Erez, J., 2021. Planktic foraminiferal Na/Ca: a potential proxy for seawater calcium concentration. Geochim. Cosmochim. Acta 305, 306–322.
- Zhou, N., Wang, Y., Ya, L., Porter, A.S., Kürschner, W.M., Li, L., Lu, N., McElwain, J.C., 2020. An inter-comparison study of three stomatal-proxy methods for CO₂ reconstruction applied to early Jurassic Ginkgoales plants. Palaeogeogr., Palaeoclimatol., Palaeoecol. 542, 109547.